

Why Rectified Power Unit Networks Fail and How to Improve It: An Effective Field Theory Perspective

Taeyoung Kim

*School of Computational Sciences
Korea Institute for Advanced Study
Seoul 02455, South Korea*

TAEYOUNGKIM@KIAS.RE.KR

Myungjoo Kang

*Department of Mathematical Science
Seoul National University
Seoul 08826, South Korea*

MKANG@SNU.AC.KR

Abstract

The Rectified Power Unit (RePU) activation function, a differentiable generalization of the Rectified Linear Unit (ReLU), has shown promise in constructing neural networks due to its smoothness properties. However, deep RePU networks often suffer from critical issues such as vanishing or exploding values during training, rendering them unstable regardless of hyperparameter initialization. Leveraging the perspective of effective field theory, we identify the root causes of these failures and propose the Modified Rectified Power Unit (MRePU) activation function. MRePU addresses RePU's limitations while preserving its advantages, such as differentiability and universal approximation properties. Theoretical analysis demonstrates that MRePU satisfies criticality conditions necessary for stable training, placing it in a distinct universality class. Extensive experiments validate the effectiveness of MRePU, showing significant improvements in training stability and performance across various tasks, including polynomial regression, physics-informed neural networks (PINNs) and real-world vision tasks. Our findings highlight the potential of MRePU as a robust alternative for building deep neural networks.

Keywords: Neural Networks, Activation Functions, Deep Learning Theory, Effective Field Theory, Rectified Power Units

1. Introduction

1.1 Activation Functions

An activation function is a function that acts on the output of each layer of a neural network. The remarkable success of deep neural networks is closely related to the choice of appropriate nonlinear activation functions, and there has been extensive discussion solely on the research of activation functions. Early studies on neural networks include the perceptron (Rosenblatt (1958)), where the activation function is the sign function, and it was composed of only one or two layers. The perceptron had the drawback that its derivative was almost everywhere zero, making it difficult to apply the backpropagation algorithm. According to (Cybenko (1989)), for a neural network to satisfy the universal approximation property, the activation function must be bounded, non-constant, monotonically increasing, and continuous. In the 1980s and 1990s, smooth activations like the sigmoid activation and tanh activation, along with their variations, were proposed (Rumelhart et al. (1986), Narayan (1997), LeCun et al. (2002)). These activations had the disadvantage of gradient vanishing when stacking layers deeply. To overcome this drawback, the Rectified Linear Unit (ReLU) was proposed by

(Nair and Hinton (2010)), whose derivative is a non-zero constant. Variations of ReLU, such as PReLU, GELU, and ELU, have also been proposed in the 2010s (He et al. (2015), Hendrycks and Gimpel (2016), Clevert et al. (2015)). Recently, there have been attempts to find activations tailored to specific tasks to impart inductive bias to the neural network structure according to the task (Ramachandran et al. (2017), Sun et al. (2024)).

1.2 Rectified Power Unit

One of the attempts to provide good regularity and inductive bias to the architecture is the Rectified Power Unit (RePU), a generalization of ReLU (Li et al. (2020)). Early results using RePU include the application of ReQU, a type of RePU, in the DeepRitz method, which is a neural network approach for solving Partial Differential Equations (PDEs) (E and Yu (2018)). RePU has also been proposed to construct differentiable neural networks, and error bounds related to this have been analyzed (Li et al. (2020)). According to research, using a RePU network allows for the optimal approximation of smooth functions in Sobolev space with optimal depth and width, and the optimal approximation error bound is also provided in Li et al. (2020). Similarly, another study derived that a shallow RePU network can approximate multivariate functions of a certain function class with finite neural network weight norms and possibly unbounded width (Abdeljawad and Grohs (2022)). Furthermore, it was shown that the derivatives of a network composed of RePU can be expressed as a mixture of various types of RePU, and an improved upper bound on the complexity of these derivatives was derived. This demonstrates the capability of RePU by showing the risk bound for the deep score matching estimator (DSME) (Shen et al. (2023)). Despite these results highlighting the good regularity of RePU neural networks, experimental evidence shows that RePU networks suffer from exploding or vanishing values and fail to train properly when the layers are deep.

1.3 Effective Field Theory of Neural Networks

The language of quantum field theory (QFT) is useful for analyzing systems with a very high degree of freedom. One such example is artificial neural networks. It is known that the distribution of neural network ensembles follows a Gaussian process when the width is infinite, corresponding to the free field in the QFT framework (Neal (1996), Rasmussen (2004), Roberts et al. (2022), Banta et al. (2024), Halverson et al. (2021)). In practice, neural networks with finite width exhibit non-Gaussianity in their distributions as layers are stacked, allowing the distribution of neurons to be calculated perturbatively, as in weakly-interacting theory (Banta et al. (2024), Halverson et al. (2021)). Interestingly, when the width of the neural network is finite, the propagation of information through the neural network can be understood as a renormalization group (RG) flow. By analyzing the recursive relations of the kernels in RG flow, hyperparameters can be tuned to a criticality state that ensures the stability of the network (Roberts et al. (2022)). Additionally, this analysis allows for the classification of activation functions into universality classes based on the behavior of the RG flow (Roberts et al. (2022)). Some types of activation functions, according to this classification, cannot satisfy criticality conditions from the outset.

1.4 Our Contribution

This paper provides a comprehensive analysis of the Rectified Power Unit (RePU) activation function and its limitations through the lens of effective field theory. Based on these insights, we propose the Modified Rectified Power Unit (MRePU) activation function, which addresses the drawbacks of RePU while preserving its advantages. Our contributions are summarized as follows:

- **Theoretical Analysis of RePU’s Limitations:** We derive the susceptibility of RePU activations and demonstrate that they fail to satisfy criticality conditions, leading to instability in deep neural networks. This analysis identifies why RePU networks experience vanishing or exploding kernels during forward propagation, irrespective of hyperparameter initialization.
- **Proposal of MRePU:** Based on our theoretical insights, we propose the Modified Rectified Power Unit (MRePU) activation function. MRePU retains the differentiability and universal approximation properties of RePU while overcoming its instability issues. We show that MRePU belongs to a distinct universality class, satisfying criticality conditions necessary for stable training.
- **Approximation Properties of MRePU Networks:** We theoretically prove that MRePU networks possess universal approximation properties for differentiable functions, akin to RePU networks. Furthermore, MRePU networks exhibit efficient polynomial approximation.
- **Experimental Validation and Inductive Bias:** Extensive experiments validate the theoretical predictions, demonstrating that MRePU introduces a specific inductive bias suitable for tasks requiring smooth approximations and accurate differentiation. While MRePU does not universally outperform ReLU or GELU across all tasks, it shows superior performance in approximating derivatives and achieving stable learning in tasks involving polynomial and differentiable function approximation. For example, MRePU networks provide meaningful improvements in training stability and accuracy for deep architectures, including those applied to physics-informed neural networks (PINNs).
- **Proposal of Criticality Condition for Hyperparameters and Empirical Validation with Real-World Tasks:** Based on our theoretical findings, we derived the criticality condition required for the statistical distribution of the initial ensemble of MRePU networks to ensure stable training. We empirically verified, by constructing phase diagrams, that this condition serves as the determinant boundary between training success and failure. Furthermore, we confirmed the effective performance of MRePU networks on real-world tasks, such as MNIST and CIFAR-10, employing widely adopted deep architectures including ResNet.

2. Preliminary

In this section, we define the neural network and activation functions that will be the subject of our analysis, focusing particularly on the Rectified Power Unit (RePU). Additionally, we explore the effective field theory of neural networks, which will be the primary tool for our analysis.

2.1 Overview of Neural Networks and Activation Functions

We primarily deal with neural networks having a fully connected network (FCN) architecture in this paper. An FCN is composed of affine transformations with hyperparameters weights and biases at each layer, followed by a nonlinear activation function applied component-wise. Specifically, it is structured as defined below:

Definition 1 (Fully Connected Network (FCN)). A Fully Connected Network $f(x; \theta) : \mathbb{R}^{n_{in}} \rightarrow \mathbb{R}^{n_{out}}$ is defined by the following recursive equations:

$$\begin{aligned} z_i^{(1)}(x_\alpha) &:= \sum_{j=1}^{n_0} W_{ij}^{(1)} x_{j;\alpha} + b_i^{(1)}, \quad \text{for } i = 1, \dots, n_1, \\ z_i^{(l+1)}(x_\alpha) &:= \sum_{j=1}^{n_l} W_{ij}^{(l+1)} \sigma(z_j^{(l)}(x_\alpha)) + b_i^{(l+1)}, \quad \text{for } i = 1, \dots, n_{l+1}; \\ l &= 1, \dots, L-1. \end{aligned} \tag{1}$$

where n_{in} is the input dimension of the neural network, n_{out} is the output dimension of the neural network, and each n_l is the width (i.e., the number of nodes at the l -th layer). L is the depth of stacked layers. The parameters $(b_i^{(l)})_{i=1, \dots, n_l}$, $(W_{ij}^{(l)})_{i=1, \dots, n_l, j=1, \dots, n_{l-1}}$ are bias vectors and weight matrices, respectively. $z_i^{(l)}$ is called the **preactivation at the l -th layer**. $\sigma : \mathbb{R} \rightarrow \mathbb{R}$ is an **activation function** that acts on each node of the preactivations.

In the previous definition of neural networks, we also explained what an activation function is. The connections between the nodes of a neural network can be seen as a type of graph, and this graph representing the connections of the neural network is called the **architecture**. Besides the architecture, there are several factors that determine the properties of a neural network (training dynamics, inductive bias, approximation properties, etc.). In this paper, we focus on the initialization of the weight and bias parameters and the activation function.

Definition 2 (Initialization distribution of biases and weights). In the definition of neural networks, there are adjustable weights and biases parameters. The method of setting these parameters at the beginning of training is called **initialization**, and typically, each parameter follows a specific probability distribution, referred to as the **initialization distribution**. Although it is possible to use mathematically complex initialization distributions, it is common practice to assign each weight and bias under the condition of being independent and identically distributed (i.i.d). The probability distributions used can include Gaussian distribution, truncated Gaussian distribution, uniform distribution, and others. For wide neural networks, it is known that when the mean of the weight distribution is 0 and the variance is constant, differences arising from different types of distributions are suppressed by $\frac{1}{\text{width}}$. Therefore, for the sake of convenience in our discussion, we will set

the distributions of weights and biases to follow a mean-zero Gaussian distribution:

$$\begin{aligned}\mathbb{E}[b_i^{(l)} b_j^{(l)}] &= \delta_{ij} C_b^{(l)} \\ \mathbb{E}[W_{i_1 j_1}^{(l)} W_{i_2 j_2}^{(l)}] &= \delta_{i_1 i_2} \delta_{j_1 j_2} \frac{C_W^{(l)}}{n_{l-1}}.\end{aligned}\tag{2}$$

where the set of bias variances $\{C_b^{(1)}, \dots, C_b^{(L)}\}$ and the set of rescaled weight variances $\{C_W^{(1)}, \dots, C_W^{(L)}\}$ are called initialization hyperparameters.

Activation functions Since the inception of artificial neural networks, various types of activation functions have been proposed. An activation function is essentially a 1D real scalar-valued function that acts on the preactivation, which is the output of a node. Because the capabilities of a neural network are greatly influenced by the type of activation function used, extensive research has been conducted in this area. We provide a brief summary of the activation functions proposed so far through Table 1.

Name	Formula	References
Perceptron	$\sigma(z) = \begin{cases} 1, & \text{if } z \geq 0 \\ 0, & \text{if } z < 0 \end{cases}$	Rosenblatt (1958)
Sigmoid	$\sigma(z) = \frac{1}{1+e^{-z}}$	Cybenko (1989)
Tanh	$\sigma(z) = \tanh(z) = \frac{e^z - e^{-z}}{e^z + e^{-z}}$	Cybenko (1989), LeCun et al. (2002)
Sin	$\sigma(z) = \sin(z)$	Parascandolo et al. (2016), Sitzmann et al. (2020)
ReLU	$\sigma(z) = \begin{cases} z, & \text{if } z \geq 0 \\ 0, & \text{if } z < 0 \end{cases}$	Nair and Hinton (2010), Glorot et al. (2011)
Leaky ReLU	$\sigma(z) = \begin{cases} z, & \text{if } z \geq 0 \\ \alpha z, & \text{if } z < 0 \end{cases}$	He et al. (2015), Maas et al. (2013)
Softplus	$\sigma(z) = \log(1 + e^z)$	Bishop (2006)
SWISH	$\sigma(z) = \frac{z}{1+e^{-z}}$	Ramachandran et al. (2017)
GELU	$\sigma(z) = \left[\frac{1}{2} + \frac{1}{2} \text{erf}\left(\frac{z}{\sqrt{2}}\right) \right] z$	Hendrycks and Gimpel (2016)

Table 1: Various Kinds of Activation functions

Now we define the RePU activation functions, which are the main objective of our work.

Definition 3 (Rectified Power Unit (RePU)). The RePU activation function is defined by the following equation:

$$\sigma(z) = \begin{cases} z^p, & \text{if } z \geq 0 \\ 0, & \text{if } z < 0 \end{cases}.$$

where p is a positive integer that determines the power to which the input z is raised. When $p = 1$, it corresponds to ReLU, and thus RePU can be considered a generalized version of ReLU. The cases where $p = 2$ and $p = 3$ are referred to as Rectified Quadratic Unit (ReLU) and Rectified Cubic Unit (ReCU), respectively. For RePU with $p = k$, it is easy to see that it is differentiable $k - 1$ times, and this property ensures that the neural network and its gradients are differentiable functions.

2.2 Effective Field Theory for Neural Networks

We utilize the framework of effective field theory to understand the distribution of pre-activations in a neural network ensemble sampled from the initialization distribution. To accomplish this, we first define the necessary concepts.

Definition 4 (M-point correlators). The moments or M -point correlators of a probability distribution $p(z) = p(z_1, \dots, z_N)$ are defined as follows:

$$\mathbb{E}[z_{\mu_1} \cdots z_{\mu_M}] = \int z_{\mu_1} \cdots z_{\mu_M} p(z) d\nu(z).$$

The collection of all M -point correlators fully characterizes the probability distribution since the information from the M -point correlators allows us to compute the expected values of analytic observables. For a Gaussian distribution, it is important to note that the distribution's information can be fully specified by the 1-point correlator (mean) and the 2-point correlator (variance). Keeping this in mind, we slightly modify the M -point correlator to define what is known as the connected correlator (also known as cumulant). The definition is as follows:

Definition 5 (M-point connected correlators). For $2 \leq M$, the cumulant or M -point connected correlators of a probability distribution $p(z)$ are defined as follows:

$$\mathbb{E}[z_{\mu_1} \cdots z_{\mu_M}]|_{\text{connected}} = \mathbb{E}[z_{\mu_1} \cdots z_{\mu_M}] - \sum_{\substack{\text{all subdivisions of } (\mu_1, \dots, \mu_M)}} \mathbb{E}[z_{\mu_{i_1,1}} \cdots z_{\mu_{i_1,j_1}}]|_{\text{connected}} \cdots \mathbb{E}[z_{\mu_{i_k,1}} \cdots z_{\mu_{i_k,j_k}}]|_{\text{connected}}.$$

Proposition 6 (Wick contraction). Suppose (X_1, \dots, X_n) is a zero-mean multivariate normal random vector. Then, all odd-order correlators vanish, and the even-order correlators are given by

$$\mathbb{E}[X_{j_1}^{i_1} \cdots X_{j_n}^{i_n}] = \sum_{(\text{all possible parings})} \prod_{(\text{parings})} \mathbb{E}[X_{p_1} X_{p_2}]$$

For $M = 1$, the connected correlator coincides with the regular correlator. For parity-symmetric distributions, it also coincides for $M = 2$. Using Wick contraction, it is known that for a Gaussian distribution, the connected correlators for $M > 2$ are zero. Therefore, higher-point connected correlators can be used to determine how much the distribution deviates from a Gaussian distribution. Additionally, if the connected correlators for $M > 2$ are small, the distribution is defined as **nearly-Gaussian**. In quantum field theory, the 2-point connected correlator can be seen as an expression of the translational symmetry of a free field. In a free field, there is no interaction due to potential, so all connected correlators higher than the 2-point vanish. Conversely, if there are interactions between particles due to a potential, higher-order connected correlators become non-zero. Similarly, in the neural network we analyze, if the higher-order correlators do not vanish and instead show significant values, this implies meaningful interactions between nodes in the feature space, suggesting that feature learning is taking place.

Using these concepts, we can analyze the probability distribution of the preactivations of an ensemble following the initialization distribution. Specifically, since each layer depends

on the previous layer, marginalization reveals that there are recursive relations between the statistics of the probability distributions of the layers.

Induced distributions Following the notation in (1), let $p(z^{(l)}|\mathcal{D})$ denote the probability distribution of the preactivations in the l -th layer given a dataset $\mathcal{D} = \{x_{i;\alpha}\}_{i=1,\dots,n_0; \alpha=1,\dots,N_{\mathcal{D}}}$. Here, α denotes the label index for the samples. For the first layer, the preactivation has $M > 2$ connected correlators equal to 0, and has the following mean and covariance, indicating that each preactivation follows an independent Gaussian distribution.

$$\begin{aligned}\mathbb{E}[z_{i;\alpha}^{(1)}] &= \mathbb{E}\left[b_i^{(1)} + \sum_{j=1}^{n_0} W_{ij}^{(1)} x_{j;\alpha}\right] = 0, \\ \mathbb{E}[z_{i_1;\alpha_1}^{(1)} z_{i_2;\alpha_2}^{(1)}] &= \mathbb{E}\left[\left(b_{i_1}^{(1)} + \sum_{j=1}^{n_0} W_{i_1 j_1}^{(1)} x_{j_1;\alpha_1}\right) \left(b_{i_2}^{(1)} + \sum_{j=1}^{n_0} W_{i_2 j_2}^{(1)} x_{j_2;\alpha_2}\right)\right] \\ &= \delta_{i_1 i_2} \left(C_b^{(1)} + C_W^{(1)} \frac{1}{n_0} \sum_{j=1}^{n_0} x_{j;\alpha_1} x_{j;\alpha_2}\right) = \delta_{i_1 i_2} G_{\alpha_1 \alpha_2}^{(1)}.\end{aligned}$$

Where $G_{\alpha_1 \alpha_2}^{(1)}$ is called as the **metric**, which represents the two-point correlator of the preactivations for different samples. Similarly, the conditional probability $p(z^{(l+1)}|z^{(l)})$ is also described by Gaussian distribution with covariance $\hat{G}_{\alpha_1 \alpha_2}^{(l+1)}$, where the distribution (i.e. $\hat{G}_{\alpha_1 \alpha_2}^{(l+1)}$) depends on the condition $z^{(l)}$. We refer to this $\hat{G}_{\alpha_1 \alpha_2}^{(l+1)}$ as the **$l+1$ -th layer stochastic metric**. We can consider the mean metric $G_{\alpha_1 \alpha_2}^{(l+1)}$, which is the average of the stochastic metric. Additionally, we can consider the variance of $\Delta \hat{G}_{\alpha_1 \alpha_2}^{(l+1)} = \hat{G}_{\alpha_1 \alpha_2}^{(l+1)} - G_{\alpha_1 \alpha_2}^{(l+1)}$, which is the fluctuation of the stochastic metric around the mean metric. We refer to scaled quantity of this variance as the **four-point vertex**, defined as follows:

$$V_{(\alpha_1 \alpha_2)(\alpha_3 \alpha_4)}^{(l+1)} := n_l \mathbb{E}\left[\Delta \hat{G}_{\alpha_1 \alpha_2}^{(l+1)} \Delta \hat{G}_{\alpha_3 \alpha_4}^{(l+1)}\right] = n_l \left(\mathbb{E}\left[\hat{G}_{\alpha_1 \alpha_2}^{(l+1)} \hat{G}_{\alpha_3 \alpha_4}^{(l+1)}\right] - G_{\alpha_1 \alpha_2}^{(l+1)} G_{\alpha_3 \alpha_4}^{(l+1)}\right).$$

The four-point vertex is related to the 4-point connected correlator as follows:

$$\begin{aligned}\mathbb{E}[z_{i_1;\alpha_1}^{(l+1)} z_{i_2;\alpha_2}^{(l+1)} z_{i_3;\alpha_3}^{(l+1)} z_{i_4;\alpha_4}^{(l+1)}]|_{\text{connected}} \\ = \frac{1}{n_l} [\delta_{i_1 i_2} \delta_{i_3 i_4} V_{(\alpha_1 \alpha_2)(\alpha_3 \alpha_4)}^{(l+1)} + \delta_{i_1 i_3} \delta_{i_2 i_4} V_{(\alpha_1 \alpha_3)(\alpha_2 \alpha_4)}^{(l+1)} + \delta_{i_1 i_4} \delta_{i_2 i_3} V_{(\alpha_1 \alpha_4)(\alpha_2 \alpha_3)}^{(l+1)}].\end{aligned}\tag{3}$$

The quantities we have just defined contain significant information about the distribution of the preactivation $p(z^{(l)}|\mathcal{D})$. If we define the action S of $p(z^{(l)}|\mathcal{D})$ as follows (parity symmetry can be easily checked):

$$\begin{aligned}S(z^{(l)}) &:= \frac{1}{2} \sum_{i=1}^{n_l} \sum_{\alpha_1 \alpha_2 \in \mathcal{D}} g_{(l)}^{\alpha_1 \alpha_2} z_{i;\alpha_1}^{(l)} z_{i;\alpha_2}^{(l)} \\ &\quad - \frac{1}{8} \sum_{i_1, i_2=1}^{n_l} \sum_{\alpha_1, \dots, \alpha_4 \in \mathcal{D}} v_{(l)}^{(\alpha_1 \alpha_2)(\alpha_3 \alpha_4)} z_{i_1;\alpha_1}^{(l)} z_{i_2;\alpha_2}^{(l)} z_{i_3;\alpha_3}^{(l)} z_{i_4;\alpha_4}^{(l)} + O((z^{(l)})^6).\end{aligned}$$

It is known that the following relationship holds for the coefficients. This can be derived by comparing the coefficients of the connected correlator given by the mean metric and

four-point vertex with those of the connected correlator assumed by the ansatz provided by action S . $g_{(l+1)}^{\alpha_1\alpha_2}$ and $v_{(l+1)}^{(\alpha_1\alpha_2)(\alpha_3\alpha_4)}$ (Roberts et al. (2022)):

$$g_{(l)}^{\alpha_1\alpha_2} = G_{(l)}^{\alpha_1\alpha_2} + O\left(\frac{1}{n_{l-1}}\right),$$

$$v_{(l)}^{(\alpha_1\alpha_2)(\alpha_3\alpha_4)} = \frac{1}{n_l} V_{(l)}^{(\alpha_1\alpha_2)(\alpha_3\alpha_4)} + O\left(\frac{1}{n_{l-1}^2}\right).$$

Where, $G_{(l)}^{\alpha_1\alpha_2}$ is inverse of mean metric $G_{\alpha_1\alpha_2}^{(l)}$ and $V_{(l)}^{(\alpha_1\alpha_2)(\alpha_3\alpha_4)}$ is defined as follows:

$$V_{(l)}^{(\alpha_1\alpha_2)(\alpha_3\alpha_4)} := \sum_{\beta_1, \dots, \beta_4 \in \mathcal{D}} G_{(l)}^{\alpha_1\beta_1} G_{(l)}^{\alpha_2\beta_2} G_{(l)}^{\alpha_3\beta_3} G_{(l)}^{\alpha_4\beta_4} V_{(\alpha_1\alpha_2)(\alpha_3\alpha_4)}^{(l)}.$$

Kernels and Representation Group flow Now, we will investigate how the statistics of the preactivation change as they pass through the layers. We will refer to the evolution of the distribution through the layers as the **representation group flow**, following the terminology of (Roberts et al. (2022)). While it is not feasible to explicitly calculate the statistics for a complex non-Gaussian distribution, it is possible to develop a perturbative theory to understand the recursive flow of the key statistics of the distribution. Before delving into this, let's define the notation for Gaussian expectations. For an observable $\mathcal{O}(z)$ with a mean-zero Gaussian distribution with variance $\mathbf{K} = (\mathbf{K}_{ij})$, the expectation is denoted as $\langle \mathcal{O}(z) \rangle_{\mathbf{K}}$. Now, if we define the **kernel** of the neural network through the following recursive relation:

$$K_{\alpha_1\alpha_2}^{(1)} := G_{\alpha_1\alpha_2}^{(1)},$$

$$K_{\alpha_1\alpha_2}^{(l+1)} = C_b^{(l+1)} + C_W^{(l+1)} \langle \sigma(z_{\alpha_1}) \sigma(z_{\alpha_2}) \rangle_{K^{(l)}}. \quad (4)$$

it is known that this kernel satisfies following properties, as discussed in (Roberts et al. (2022)).

$$G_{\alpha_1\alpha_2}^{(l)} = K_{\alpha_1\alpha_2}^{(l)} + O\left(\frac{1}{n_{l-1}}\right),$$

$$V_{(\alpha_1\alpha_2)(\alpha_3\alpha_4)}^{(l+1)} = \left(C_W^{(l+1)}\right)^2 \left[\langle \sigma(z_{\alpha_1}) \sigma(z_{\alpha_2}) \sigma(z_{\alpha_3}) \sigma(z_{\alpha_4}) \rangle_{K^{(l)}} \right. \\ \left. - \langle \sigma(z_{\alpha_1}) \sigma(z_{\alpha_2}) \rangle_{K^{(l)}} \langle \sigma(z_{\alpha_3}) \sigma(z_{\alpha_4}) \rangle_{K^{(l)}} \right] \\ + \frac{n_l}{4n_{l-1}} \sum_{\beta_1, \dots, \beta_4 \in \mathcal{D}} V_{(l)}^{(\alpha_1\alpha_2)(\alpha_3\alpha_4)} \left\langle \sigma(z_{\alpha_1}) \sigma(z_{\alpha_2}) \left(z_{\beta_1} z_{\beta_2} - K_{\beta_1\beta_2}^{(l)} \right) \right\rangle_{K^{(l)}} \\ \times \left\langle \sigma(z_{\alpha_3}) \sigma(z_{\alpha_4}) \left(z_{\beta_3} z_{\beta_4} - K_{\beta_3\beta_4}^{(l)} \right) \right\rangle_{K^{(l)}} + O\left(\frac{1}{n_l}\right). \quad (5)$$

Susceptibility When expanding the kernel matrix for two inputs $(x_{i;+})$ and $(x_{i;-})$, it can be written as follows:

$$K^{(l)} = \begin{pmatrix} K_{++}^l & K_{+-}^l \\ K_{-+}^l & K_{--}^l \end{pmatrix} = K_{[0]}^{(l)} \begin{pmatrix} 1 & 1 \\ 1 & 1 \end{pmatrix} + K_{[1]}^{(l)} \begin{pmatrix} 1 & 0 \\ 0 & -1 \end{pmatrix} + K_{[2]}^{(l)} \begin{pmatrix} 1 & -1 \\ -1 & 1 \end{pmatrix}.$$

Where, $K_{\pm\pm}^{(l)} := \mathbb{E}\left[\frac{1}{n_l} \sum_{i=1}^{n_l} (z_{i;\pm}^{(l)})^2\right]$, $K_{\pm\mp}^{(l)} := \mathbb{E}\left[\frac{1}{n_l} \sum_{i=1}^{n_l} z_{i;\pm}^{(l)} z_{i;\mp}^{(l)}\right]$ The coefficients $K_{[\alpha]}^{(l)}$ are given by:

$$\begin{aligned} K_{[0]}^{(l)} &= \frac{1}{4}[K_{++}^{(l)} + K_{--}^{(l)} + 2K_{+-}^{(l)}], \\ K_{[1]}^{(l)} &= \frac{1}{2}[K_{++}^{(l)} - K_{--}^{(l)}], \\ K_{[2]}^{(l)} &= \frac{1}{4}[K_{++}^{(l)} + K_{--}^{(l)} - 2K_{+-}^{(l)}]. \end{aligned}$$

If we express $(x_{i;+})$ and $(x_{i;-})$ as $x_{i;\pm} = \frac{x_{i;+} + x_{i;-}}{2} \pm \delta x_i$, it can be seen that as (δx_i) approaches zero, the coefficients $K_{[1]}^{(l)}, K_{[2]}^{(l)}$ also approach zero. Consequently, the coefficients can be expanded as follows:

$$\begin{aligned} K_{[0]}^{(l)} &= K_{00}^{(l)} + \delta^2 K_{[0]}^{(l)} + O(\delta^4), \\ K_{[1]}^{(l)} &= \delta K_{[1]}^{(l)} + \delta^3 K_{[1]}^{(l)} + O(\delta^5), \\ K_{[2]}^{(l)} &= \delta^2 K_{[2]}^{(l)} + \delta^4 K_{[2]}^{(l)} + O(\delta^6). \end{aligned}$$

Then, it is known that the following recursion can be derived (Roberts et al. (2022)):

$$\begin{aligned} K_{00}^{(l+1)} &= C_b + C_W g(K_{00}^{(l)}), \\ \delta K_{[1]}^{(l+1)} &= \mathcal{X}_{\parallel}(K_{00}^{(l)}) \delta K_{[1]}^{(l)}, \\ \delta^2 K_{[2]}^{(l+1)} &= \mathcal{X}_{\perp}(K_{00}^{(l)}) \delta^2 K_{[2]}^{(l)} + h(K_{00}^{(l)}) (\delta K_{[1]}^{(l)})^2. \end{aligned}$$

Where $K_{00}^{(l+1)}$ is the kernel for a single input, and each $g, h, \mathcal{X}_{\parallel}, \mathcal{X}_{\perp}$ are defined as follows:

$$\begin{aligned} g(K) &:= \langle \sigma(z) \sigma(z) \rangle_K, \\ \mathcal{X}_{\parallel}(K) &:= C_W g'(K) = \frac{C_W}{K} \langle z \sigma'(z) \sigma(z) \rangle_K, \\ \mathcal{X}_{\perp}(K) &:= C_W \langle \sigma'(z) \sigma'(z) \rangle_K, \\ h(K) &:= \frac{C_W}{4K^2} \left\langle \sigma'(z) \sigma'(z) (z^2 - K) \right\rangle_K = \frac{1}{2} \frac{d}{dK} \mathcal{X}_{\perp}(K). \end{aligned} \tag{6}$$

$K_{[1]}^{(l)}$ and $K_{[2]}^{(l)}$ represent the difference in the squared distances between two inputs and a value related to the square of the difference between the two inputs, respectively. As the inputs become closer, their leading terms exhibit a geometric ratio in susceptibility as they pass through layers, which forms the basis for naming \mathcal{X}_{\parallel} and \mathcal{X}_{\perp} as the parallel and perpendicular susceptibility, respectively. Since each leading term follows this geometric ratio in susceptibility, if the value is less than 1, the kernel vanishes along the layer, and if it is greater than 1, it diverges. Thus, setting each susceptibility to 1 is essential for maintaining a stable kernel.

Summary of Framework In this section, we investigate the evolution of preactivation statistics across layers, referred to as the Representation Group flow. By analyzing the recursive kernel relation (Eq. (4)), we derive a fixed point for the statistical flow. When the initial ensemble of the network operates near this fixed point, the propagation of small perturbations through the layers is governed by the parallel (\mathcal{X}_{\parallel}) and perpendicular (\mathcal{X}_{\perp}) susceptibilities. These quantities can be interpreted as the eigenvalues of the linearized flow along the respective directions around the fixed point. Consequently, for both training dynamics and inference, it is crucial that these eigenvalues are close to unity ($\mathcal{X} \approx 1$). This criticality condition ensures that perturbations are neither amplified nor suppressed but are preserved across layers, thereby maintaining a stable signal propagation.

3. Failure of RePU Activation

3.1 Susceptibility Calculation

Activation functions that exhibit similar behaviors according to the RG flow are classified into **universality classes**. Universality class is a concept in statistical physics used to classify systems that exhibit similar behavior at the limit scale. According to (Roberts et al. (2022)), scale-invariant activations (e.g. ReLU, LeakyReLU) form a single universality class called the self-invariant universality class. Tanh and Sin fall into the $K^* = 0$ universality class, while SWISH and GELU belong to the half-stable universality class. On the other hand, Perceptron, Sigmoid, and Softplus are known to not satisfy criticality at all. We will now calculate the susceptibility for the RePU activation function following Eq. (6) and demonstrate that RePU also fails to satisfy criticality. For the RePU activation function of order p , the parallel susceptibility and perpendicular susceptibility are calculated as follows:

$$\begin{aligned}\mathcal{X}_{\parallel}(K) &= \frac{C_W}{K} \langle z\sigma'(z)\sigma(z) \rangle_K = \frac{C_W}{K} \langle z\lfloor pz^{p-1} \rfloor_+ \lfloor z^p \rfloor_+ \rangle_K \\ &= \frac{C_W p}{K \sqrt{2\pi K}} \int_0^\infty e^{-\frac{z^2}{2K}} z^{2p} dz = \frac{C_W p (2p-1)!! K^{p-1}}{2}. \\ \mathcal{X}_{\perp}(K) &= C_W \langle \sigma'(z)\sigma'(z) \rangle_K = C_W \langle p^2 \lfloor z^{p-1} \rfloor_+ \lfloor z^{p-1} \rfloor_+ \rangle_K \\ &= \frac{C_W p^2}{\sqrt{2\pi K}} \int_0^\infty e^{-\frac{z^2}{2K}} z^{2p-2} dz = \frac{C_W p^2 (2p-3)!! K^{p-1}}{2}.\end{aligned}\tag{7}$$

Here the notation $n!!$ means double factorial (e.g. $7!! = 7 \cdot 5 \cdot 3 \cdot 1$). The parallel susceptibility to perpendicular susceptibility ratio is $2p-1 : p$. Therefore, except for $p=1$ (i.e., ReLU), it is impossible to set both susceptibilities to 1 simultaneously. If we set the parallel susceptibility to 1, the perpendicular susceptibility will be less than 1, causing the distance between two inputs to vanish as they propagate through the layers. Conversely, if we set the perpendicular susceptibility to 1, the parallel susceptibility will be greater than 1, causing each input to diverge as it propagates through the layers.

3.2 Experimental Validation

Empirical Kernel Behavior at Initialization According to the results in section 3.1, the kernel value of Neural Networks with RePU (for $p > 1$) for a single input must either

explode or vanish as it propagates through the layers under the initialization distribution. In this section, we experimentally verify this. For the experiment, the neural network is configured with an input dimension of 2, an output dimension of 1, hidden layers with widths of 512, and a depth of 10 (therefore, the total number of layers, including the input and output layers, is 12). The activation function is RePU. The initialization distribution follows Eq. (2), with C_b set to 0, and C_W adjusted during the experiment. To experimentally observe the change in the kernel, we define the following empirical kernel quantities:

$$\begin{aligned}\hat{K}^{(l)}(\Theta)|_{\mathcal{D}=x_0} &:= \frac{1}{n_l} \sum_i^{n_l} \left(z_i^{(l)}(\Theta)|_{\mathcal{D}=x_0} \right)^2 \\ \hat{K}^{(l)}(\mathcal{D})|_{\Theta=\Theta_0} &:= \frac{1}{n_l} \sum_i^{n_l} \left(z_i^{(l)}(\mathcal{D})|_{\Theta=\Theta_0} \right)^2.\end{aligned}$$

Where $z_i^{(l)}(\Theta)|_{\mathcal{D}=x_0}$ is a random variable conditioned on the input x_0 and has randomness on Θ . Similarly, $z_i^{(l)}(\mathcal{D})|_{\Theta=\Theta_0}$ is a random variable conditioned on the parameter Θ and has randomness on the data input. Each component of sample in \mathcal{D} follows $N(0, 1)$. x_0 is also generated from \mathcal{D} . The experimental results for a width of 512, $p = 2$, and $C_W = 21.3$ are shown in Figs. 1. We observed that if C_W is set smaller, the kernel vanishes on an $\mathcal{O}(\exp(\exp(-l)))$ scale, and if C_W is set larger, it explodes on an $\mathcal{O}(\exp(\exp(l)))$ scale. The results in the figure for $C_W = 21.3$ show that the kernel is highly sensitive to initial conditions and tends to either double exponentially explode or vanish. According to Eqns.(6) and (7) the susceptibility itself acts as a geometric ratio and is proportional to the kernel. As this ratio increases exponentially, it causes the kernel to grow double exponentially.

Dynamics of Mean Outputs and Kernels during Training In this section, we experimentally observe the dynamics of kernels in RePU neural networks during training. In the backpropagation algorithm used for updating network parameters, each factor in the chain rule is proportional to the perpendicular susceptibility at each layer, as described by the following equation.

$$\begin{aligned}\mathbb{E} \left[\sum_{j_1, j_2} \frac{dz_i^{(l+1)}}{dz_{j_1}^{(l)}} \frac{dz_i^{(l+1)}}{dz_{j_2}^{(l)}} \right] &= \mathbb{E} \left[\sum_{j_1, j_2} W_{ij_1}^{(l+1)} W_{ij_2}^{(l+1)} \sigma'_{j_1}^{(l)} \sigma'_{j_2}^{(l)} \right] \\ &= C_W \langle \sigma'(z) \sigma'(z) \rangle_{K^{(l)}} = C_W \mathcal{X}_{\perp}^{(l)}\end{aligned}$$

Through this, we can infer that in RePU neural networks, the kernel either increases or decreases double exponentially, and since the perpendicular susceptibility is proportional to this, the training dynamics become highly unstable or converge rapidly. To experimentally verify this, we designed an experiment using synthetic data. The task involved observing how well the neural network performs regression on synthetic data, where the input data are points in the plane (x, y) with $x \sim N(0, 1)$ and $y \sim N(0, 1)$, and the target is set to $x^2 + y^2$. The training dataset is composed of 100 samples. We conducted experiments with a network width of 512 and with 1, 3, and 5 hidden layers, testing cases where $p = 2$ and $p = 3$. The C_W values were adjusted based on the architecture; if C_W is too small, the kernel decreases double exponentially, and if C_W is too large, the kernel becomes highly unstable

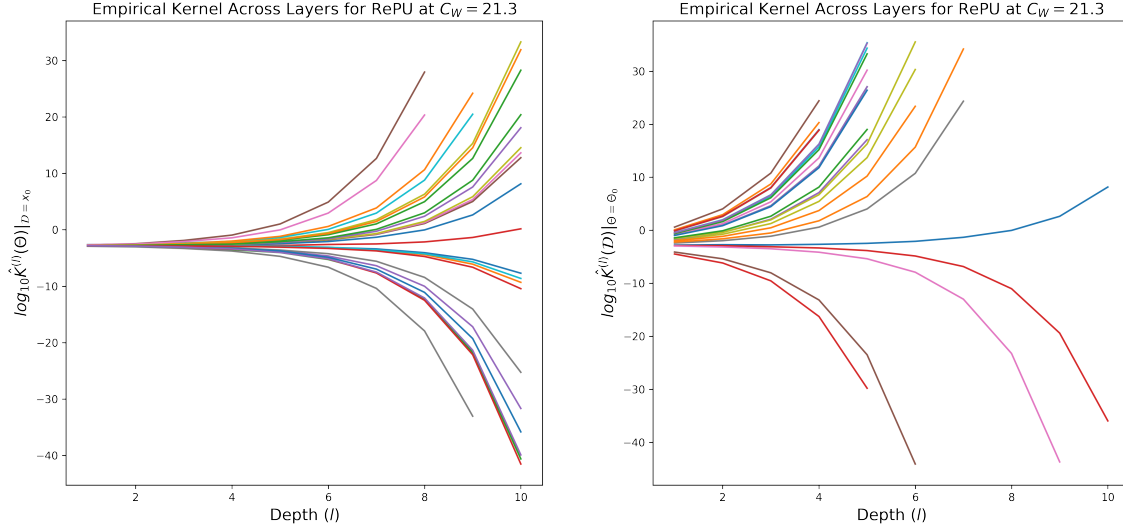


Figure 1: Empirical Kernels at Initialization Across Layers for RePU Activation with $p = 2$. **Left:** Data is fixed and randomness is in the weight parameters. **Right:** Weight parameters are fixed and data is random. Each line represents a sample.

and eventually diverges. Therefore, we experimentally determined and set an appropriate C_W value. We calculated the kernel for an ensemble of 100 neural networks, obtaining the mean and variance while excluding models where the kernel overflowed due to explosion. The results are presented in Tables 2 and 3, with the results for 5 hidden layers and $p = 2$ depicted in Fig. 2. We then tested the ensemble of 100 neural network models trained under each setting on a test dataset generated from the same distribution as the training data. The results are depicted in Fig. 3. From the aggregated results of the kernel and the mean outputs on the test dataset, we observed that significant learning only occurs when there is a single hidden layer. When the network has 3 or 5 hidden layers, the kernel values quickly diminish as the layers deepen, leading to poor learning performance. Additionally, as the depth of the network increases, the mean output converges to a constant, with its standard deviation also converging to a very small value.

(N_h, C_W)	(1, 2.5)	(3, 3.0)	(5, 2.6)
Epochs			
At initialization	$(1.39 \times 10^{-3}, 3 \times 10^{-4})$	$(1.28 \times 10^{-6}, 1.5 \times 10^{-6})$	$(6.91 \times 10^{-11}, 1.9 \times 10^{-10})$
At 250 epochs	$(1.71 \times 10^{-3}, 4 \times 10^{-4})$	$(2.80 \times 10^{-5}, 1.2 \times 10^{-5})$	$(4.29 \times 10^{-7}, 2.7 \times 10^{-7})$
At 500 epochs	$(2.71 \times 10^{-3}, 8 \times 10^{-4})$	$(7.44 \times 10^{-5}, 5.3 \times 10^{-5})$	$(1.03 \times 10^{-6}, 7.2 \times 10^{-7})$
At 750 epochs	$(4.57 \times 10^{-3}, 1.5 \times 10^{-3})$	$(1.35 \times 10^{-4}, 9.7 \times 10^{-5})$	$(1.75 \times 10^{-6}, 1.3 \times 10^{-6})$
At 1000 epochs	$(6.70 \times 10^{-3}, 1.6 \times 10^{-3})$	$(2.14 \times 10^{-4}, 1.4 \times 10^{-4})$	$(2.62 \times 10^{-6}, 2.1 \times 10^{-6})$

Table 2: Means and Standard Deviations of the Empirical Kernel at the End of Hidden Layers. Here, N_h denotes the number of hidden layers, and C_W represents hyperparameter for the variance of weight parameters at initialization. The order of RePU is 2 in this case.

(N_h, C_W)	(1, 4.5)	(3, 2.9)	(5, 2.7)
Epochs			
At initialization	$(9.01 \times 10^{-3}, 4 \times 10^{-3})$	$(3.49 \times 10^{-10}, 1.3 \times 10^{-9})$	$(1.22 \times 10^{-14}, 8.3 \times 10^{-14})$
At 250 epochs	$(1.05 \times 10^{-2}, 4 \times 10^{-3})$	$(1.34 \times 10^{-7}, 1.6 \times 10^{-7})$	$(1.54 \times 10^{-12}, 9.0 \times 10^{-12})$
At 500 epochs	$(1.14 \times 10^{-2}, 5.1 \times 10^{-3})$	$(2.30 \times 10^{-7}, 2.2 \times 10^{-7})$	$(1.91 \times 10^{-12}, 1.0 \times 10^{-11})$
At 750 epochs	$(1.24 \times 10^{-2}, 6.1 \times 10^{-3})$	$(3.31 \times 10^{-7}, 2.9 \times 10^{-7})$	$(2.35 \times 10^{-12}, 1.2 \times 10^{-11})$
At 1000 epochs	$(1.36 \times 10^{-2}, 7.5 \times 10^{-3})$	$(4.53 \times 10^{-7}, 4.0 \times 10^{-7})$	$(2.81 \times 10^{-12}, 1.5 \times 10^{-11})$

Table 3: Means and Standard Deviations of the Empirical Kernel at the End of Hidden Layers. Here, N_h denotes the number of hidden layers, and C_W represents hyperparameter for the variance of weight parameters at initialization. The order of RePU is 3 in this case.

4. Modified Rectified Power Unit (MRePU)

In this section, we propose the modified Rectified Power Unit (MRePU) function to overcome the limitations of RePU, which cannot be stacked deeply. MRePU retains the advantages of RePU (e.g., differentiability) while fundamentally addressing the existing issues. The definition of MRePU is as follows:

Definition 7 (Modified Rectified Power Unit (MRePU)). The MRePU activation function of order $p > 1$ is defined by the following equation:

$$\sigma_{m;p}(z) = \begin{cases} z(z+1)^p, & \text{if } z \geq -1 \\ 0, & \text{if } z < -1 \end{cases}.$$

Similar to RePU, the MRePU function of order p has the property of being differentiable $p-1$ times.

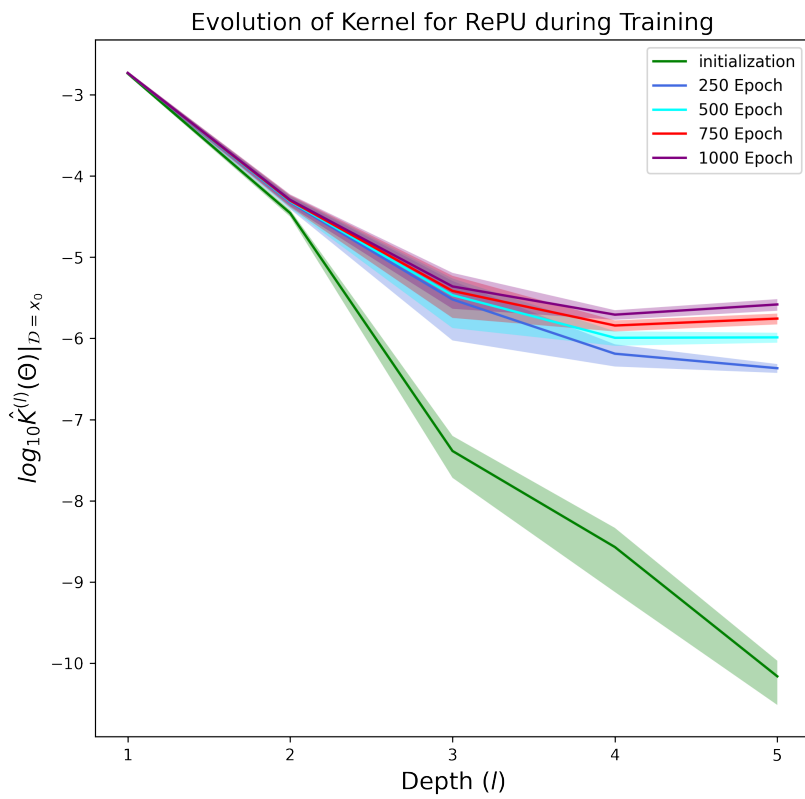


Figure 2: The evolution of the mean of empirical kernels over an ensemble of 100 models for $x_0 = (1, 0)$ as training progresses for the RePU activation with $p = 2$. The shaded areas represent the region between $\log_{10}(\text{mean} \pm 0.1 \times \text{standard deviation})$.

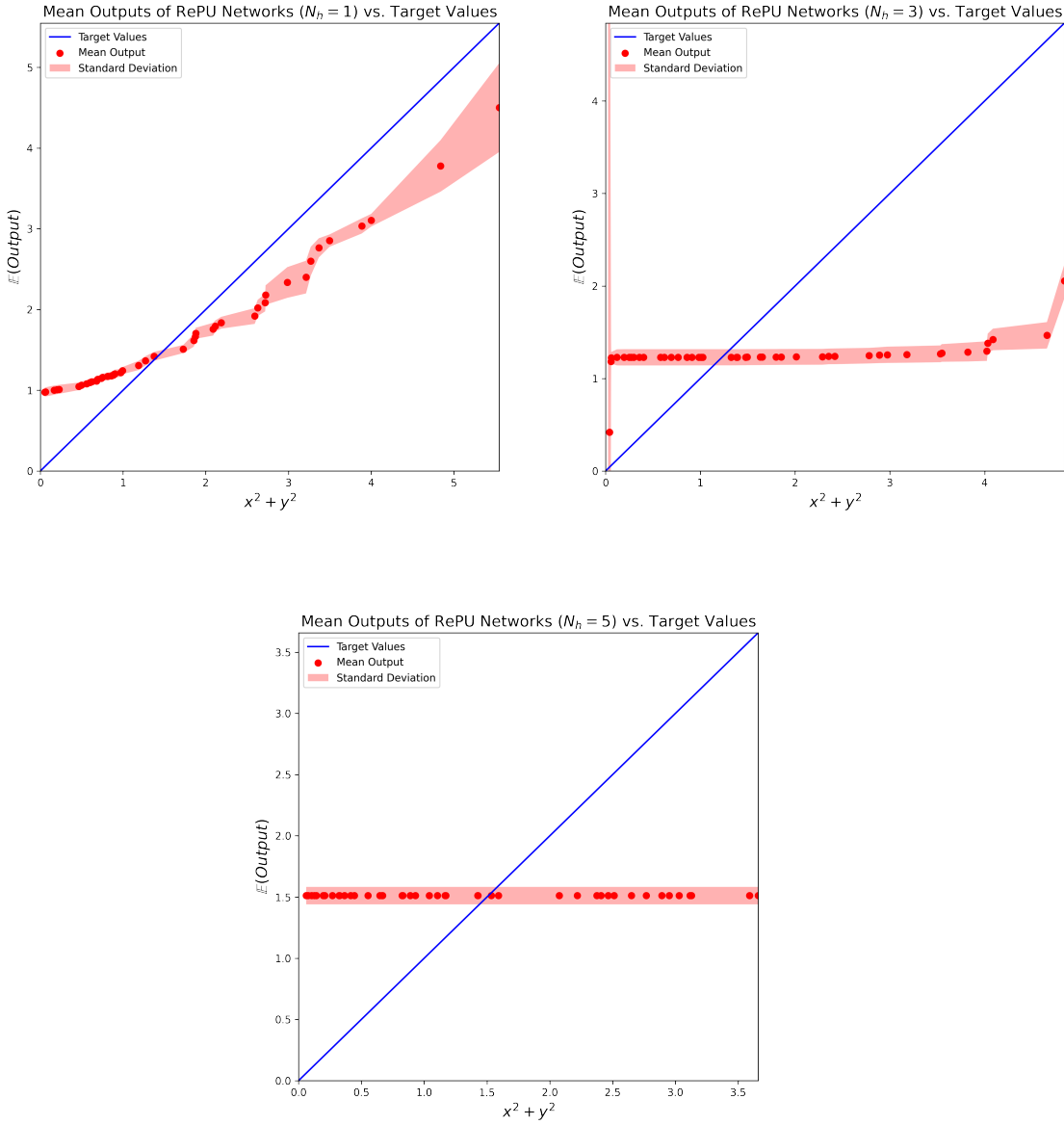


Figure 3: Mean outputs over an ensemble of 100 models versus target values on random test data. The shaded areas represent the region of 1 standard deviation. **Top left:** hidden layers (N_h)= 1, **Top right:** $N_h = 3$, **Bottom:** $N_h = 5$.

4.1 Susceptibility Calculation

We compute the parallel and perpendicular susceptibilities of the proposed MRePU activation. For an MRePU of order p , they are given by

$$\begin{aligned}\mathcal{X}_{\parallel}(K) &= \frac{C_W}{K} \langle z \sigma'(z) \sigma(z) \rangle_K = \frac{C_W}{K \sqrt{2\pi K}} \int_{-1}^{\infty} (z+1)^{2p-1} ((p+1)z+1) z^2 e^{-z^2/(2K)} dz, \\ \mathcal{X}_{\perp}(K) &= C_W \langle \sigma'(z) \sigma'(z) \rangle_K = \frac{C_W}{\sqrt{2\pi K}} \int_{-1}^{\infty} (z+1)^{2p-2} ((p+1)z+1)^2 e^{-z^2/(2K)} dz.\end{aligned}\tag{8}$$

Proposition 8. Let $\phi(t) = \frac{1}{\sqrt{2\pi}} e^{-t^2/2}$ and $I_n(\alpha) := \int_{\alpha}^{\infty} y^n \phi(y) dy$ with $\alpha = -1/\sqrt{K}$. Then

$$\begin{aligned}\mathcal{X}_{\parallel}(K) &= C_W \sum_{n=2}^{2p+2} A_n(p) K^{\frac{n}{2}-1} I_n\left(-\frac{1}{\sqrt{K}}\right), \\ \mathcal{X}_{\perp}(K) &= C_W \sum_{n=0}^{2p} B_n(p) K^{\frac{n}{2}} I_n\left(-\frac{1}{\sqrt{K}}\right),\end{aligned}\tag{9}$$

where, with the convention $\binom{m}{r} = 0$ if $r \notin \{0, \dots, m\}$,

$$A_n(p) = (p+1) \binom{2p-1}{n-3} + \binom{2p-1}{n-2}, \quad B_n(p) = (p+1)^2 \binom{2p-2}{n-2} + 2(p+1) \binom{2p-2}{n-1} + \binom{2p-2}{n}.$$

Proof. (1) *Polynomial expansion.* Write

$$(z+1)^{2p-1} ((p+1)z+1) z^2 = (p+1) \sum_{j=0}^{2p-1} \binom{2p-1}{j} z^{j+3} + \sum_{j=0}^{2p-1} \binom{2p-1}{j} z^{j+2}.$$

Collecting the z^n terms gives the coefficient in front of z^n as $A_n(p) = (p+1) \binom{2p-1}{n-3} + \binom{2p-1}{n-2}$. Similarly,

$$(z+1)^{2p-2} ((p+1)z+1)^2 = (p+1)^2 \sum_{j=0}^{2p-2} \binom{2p-2}{j} z^{j+2} + 2(p+1) \sum_{j=0}^{2p-2} \binom{2p-2}{j} z^{j+1} + \sum_{j=0}^{2p-2} \binom{2p-2}{j} z^j,$$

whence the z^n coefficient is $B_n(p) = (p+1)^2 \binom{2p-2}{n-2} + 2(p+1) \binom{2p-2}{n-1} + \binom{2p-2}{n}$.

(2) *Reduction to I_n .* For any integer $n \geq 0$, the change of variables $y = z/\sqrt{K}$ yields

$$\int_{-1}^{\infty} z^n \frac{e^{-z^2/(2K)}}{\sqrt{2\pi K}} dz = K^{n/2} \int_{-1/\sqrt{K}}^{\infty} y^n \phi(y) dy = K^{n/2} I_n\left(-\frac{1}{\sqrt{K}}\right).$$

Combining (1)–(2) and summing termwise gives the stated formulas. \square

Corollary 9 (small- K limit). As $K \rightarrow 0$,

$$\mathcal{X}_{\parallel}(K) \rightarrow C_W, \quad \mathcal{X}_{\perp}(K) \rightarrow C_W.$$

Proof. Let $\beta = 1/\sqrt{K} \rightarrow \infty$. Since $I_n(-\beta) = \int_{-\beta}^{\infty} y^n \phi(y) dy$ and ϕ is integrable with polynomial weights, dominated convergence gives

$$\lim_{\beta \rightarrow \infty} I_n(-\beta) = \int_{-\infty}^{\infty} y^n \phi(y) dy = \begin{cases} 0, & n \text{ odd}, \\ (n-1)!! & n \text{ even}. \end{cases}$$

In $\mathcal{X}_{\parallel}(K) = C_W \sum_{n=2}^{2p+2} A_n(p) K^{\frac{n}{2}-1} I_n(-\beta)$, all terms with $n > 2$ vanish because $K^{\frac{n}{2}-1} \rightarrow 0$, while for $n = 2$ we have $K^0 = 1$, $I_2(-\beta) \rightarrow 1$, and $A_2(p) = (p+1) \binom{2p-1}{-1} + \binom{2p-1}{0} = 1$. Hence $\lim_{K \rightarrow 0} \mathcal{X}_{\parallel}(K) = C_W$. Likewise, in $\mathcal{X}_{\perp}(K) = C_W \sum_{n=0}^{2p} B_n(p) K^{\frac{n}{2}} I_n(-\beta)$, the leading term is $n = 0$ with $K^0 = 1$, $I_0(-\beta) \rightarrow 1$, and $B_0(p) = (p+1)^2 \binom{2p-2}{-2} + 2(p+1) \binom{2p-2}{-1} + \binom{2p-2}{0} = 1$; all $n \geq 1$ terms vanish. Thus $\lim_{K \rightarrow 0} \mathcal{X}_{\perp}(K) = C_W$. \square

Numerics. For visualization we evaluate the above closed forms numerically. We fix $C_W = 1$ and sweep K on a logarithmic grid for $p \in \{2, 3\}$. Fig. 4 shows \mathcal{X}_{\parallel} , \mathcal{X}_{\perp} , and their ratio; as $K \rightarrow 0$, the ratio tends to 1, in agreement with the corollary and placing MRePU in the $K^* = 0$ universality class. With an appropriate choice of C_W , the kernel is kept from exploding or vanishing.

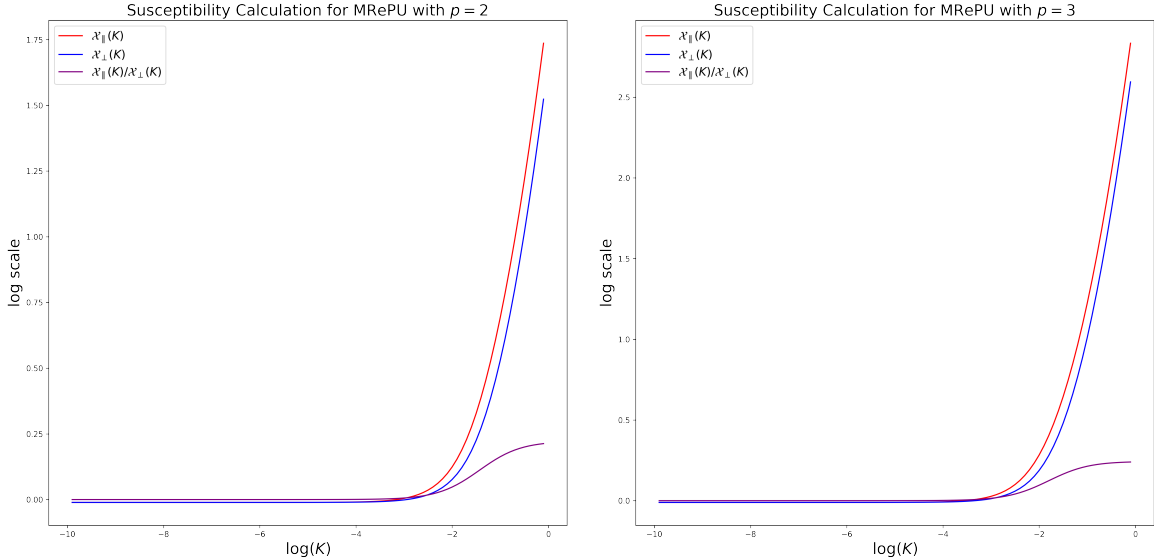


Figure 4: **Parallel and perpendicular susceptibilities and their ratio** for MRePU with $p = 2$ (left) and $p = 3$ (right), with $(C_W, C_b) = (1, 0)$. The ratio tends to 1 as $K \rightarrow 0$.

4.2 Experimental Results

Now, as we did with RePU Neural Networks, we will investigate the statistical properties of MRePU under the same experimental settings.

Empirical Kernel and Four-point Vertex Behavior at Initialization As with the RePU case, we investigate the statistical properties of the neural network ensemble given by the initialization distribution. The experimental environment remains identical to that of the RePU Networks, with the only change being the activation function, which is now MRePU with $p = 2$. The results for $C_W = 1.0$ are shown in Fig. 5. As can be seen from the graph, the empirical kernel maintains a consistent scale across both random data and weight parameters. Additionally, we also examined the behavior of the Four-point vertex for MRePU. Eq. (5) can be simplified for a single input as follows:

$$V^{(l+1)} = \mathcal{X}_{\parallel}^2(K^{(l)})V^{(l)} + C_W^2 \left[\langle \sigma^4(z) \rangle_{K^{(l)}} - \langle \sigma^2(z) \rangle_{K^{(l)}}^2 \right] + O\left(\frac{1}{n_l}\right). \quad (10)$$

Fig. 6 illustrates how the empirical four-point vertex, calculated from an ensemble of 1000 models using Eq. (3), changes across layers (with input $x_0 = (1, 0)$). \mathcal{X}_{\parallel} increases as the kernel grows, and since the kernel itself depends on C_W , the inductive change in the four-point vertex is determined by C_W according to Eq. (10). As evidence of this, the left figure shows that the four-point vertex increases more steeply as C_W becomes larger. We also investigated the behavior of the four-point vertex across different widths. The results indicate that with smaller widths, perturbative effects in Eq. (10) become more pronounced, leading to a more rapid increase in the four-point vertex, and overall, higher values are observed. The four-point vertex serves as an indicator of non-Gaussianity, which is expected to increase as more layers with non-linear activations are added. Moreover, since smaller widths imply stronger interactions between neurons, these experimental results align well with our theoretical predictions.

Dynamics of Statistics During Training Now, we will examine how the statistics of the MRePU Network ensemble change under training dynamics. The experimental setup is the same as in the case of the RePU Network, and the number of hidden layers is set to 5. In this case, we constructed the training dataset in the same way as in the RePU activation case, but the number of samples is set to 1000. Although the theoretical approximation suggests setting $C_W = 1.0$, meaningful learning was only achieved with a slightly lower value, possibly due to the perturbative effects in the MRePU Network. In our experiments, we set $C_W = 0.8$. The dynamics of the kernel and four-point vertex are depicted in Fig. 7, while the comparison of the ensemble's mean output against the target for the test dataset is shown in Fig. 8. Surprisingly, we observed that even with a vanilla FCN (Fully Connected Network) without considering architectures like ResNet, which are designed to prevent issues like the vanishing gradient, the deep neural network with 5 hidden layers still achieved meaningful learning using the MRePU function we designed. Additionally, as shown on the left side of Fig. 7, we also calculated the perpendicular susceptibility, which showed a tendency to approach 1 as training progressed. On the right side of the same figure, it can be seen that the ensemble's four-point vertex decreases to 0 during initialization but tends to increase linearly with the layers as training progresses. An increasing four-point vertex indicates growing interactions between neurons, which implies that representation learning is occurring. This suggests that the deep vanilla MRePU network is indeed engaging in meaningful representation learning.

Hyperparameter Criteria from Kernel Analysis Our kernel-based analysis yields concrete guidelines for configuring MRePU networks to achieve training stability. First, as

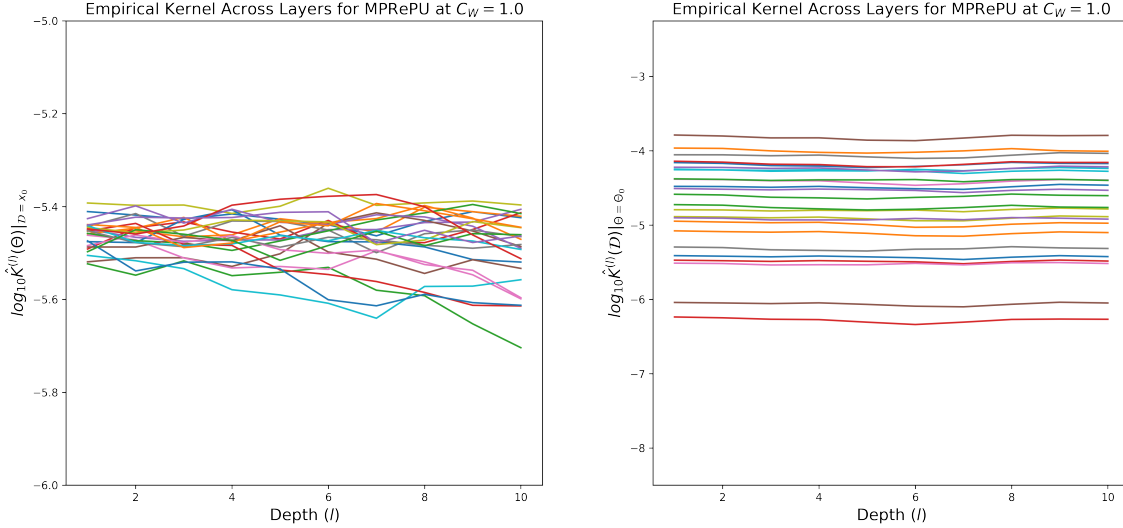


Figure 5: Empirical Kernels at Initialization Across Layers for MRePU Activation with $p = 2$. **Left:** Data is fixed and randomness is in the weight parameters. **Right:** Weight parameters are fixed and data is random. Each line represents a sample.

implied by Corollary 9 and Eq. (4), MRePU belongs to the $K^* = 0$ universality class. Consequently, the input (and hence the induced kernel scale) must be sufficiently small for the kernel magnitude to remain steady as depth increases. Next, fixing K at a suitably small value, Eq. (9) shows that choosing

$$C_W \simeq \frac{1}{\sum_{n=2}^{2p+2} A_n(p) K^{\frac{n}{2}-1} I_n\left(-\frac{1}{\sqrt{K}}\right)} \simeq \frac{1}{\sum_{n=0}^{2p} B_n(p) K^{\frac{n}{2}} I_n\left(-\frac{1}{\sqrt{K}}\right)}. \quad (11)$$

guarantees a stable kernel at initialization in theory. We validate the practical effectiveness of these criteria on real-world datasets—MNIST and CIFAR-10—in Section 5.3.

5. Approximation Properties of MRePU networks

In this section, we provide a theoretical justification that neural networks equipped with the MRePU activation can reconstruct polynomials, in close analogy to RePU networks, and consequently inherit the same universal approximation property for the class of differentiable functions established in Shen et al. (2023). Beyond this theoretical guarantee, we empirically demonstrate that MRePU networks exhibit a suitable inductive bias when approximating certain function classes. Furthermore, we show through experiments on standard benchmarks such as MNIST and CIFAR-10 that, under the proposed criticality condition, training remains stable and reliably converges.

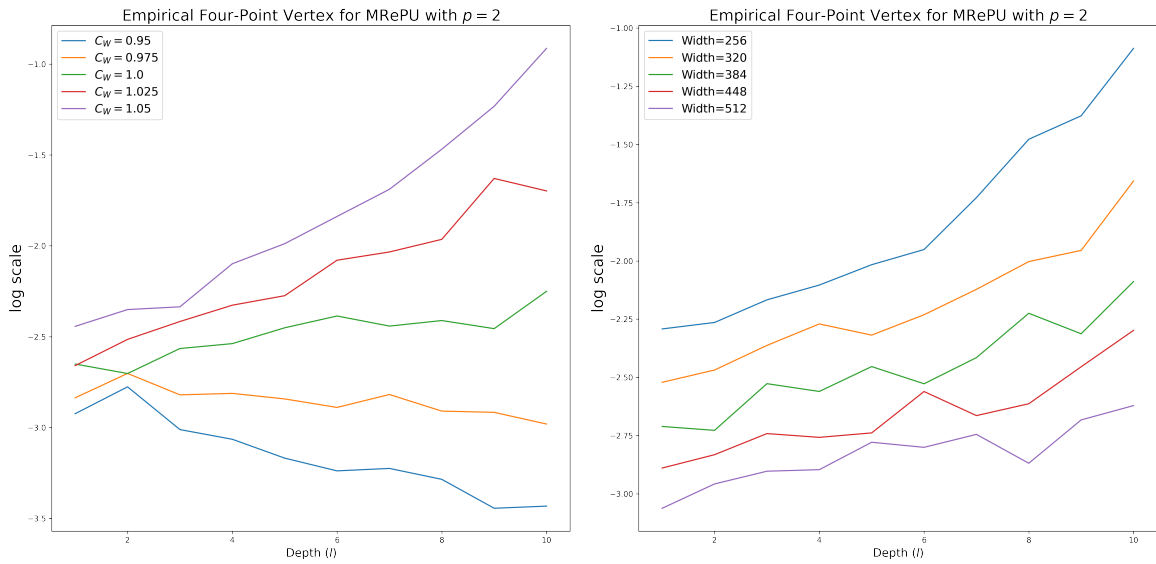


Figure 6: Empirical Four-Point Vertex Across Layers at Initialization. Each value is calculated over an ensemble of 1000 models. **Left:** Width is fixed at 512, and C_W is varying. **Right:** C_W is fixed at 1.0, and the width is varying.

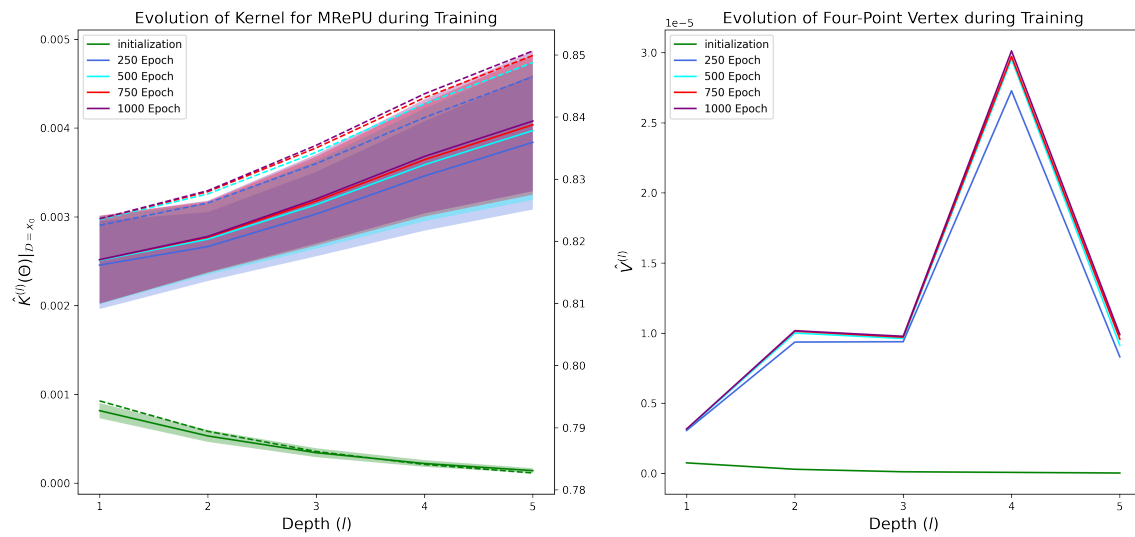


Figure 7: The evolution of the mean of empirical kernels (solid line, left y-axis) and perpendicular susceptibility (dotted line, right y-axis) (**Left**) and the four-point vertex (**Right**) over an ensemble of 100 models for $x_0 = (1, 0)$ as training progresses for the MRePU activation with $p=2$. The shaded areas represent the region between $\log_{10}(\text{mean} \pm \text{standard deviation})$ (for **Left**).

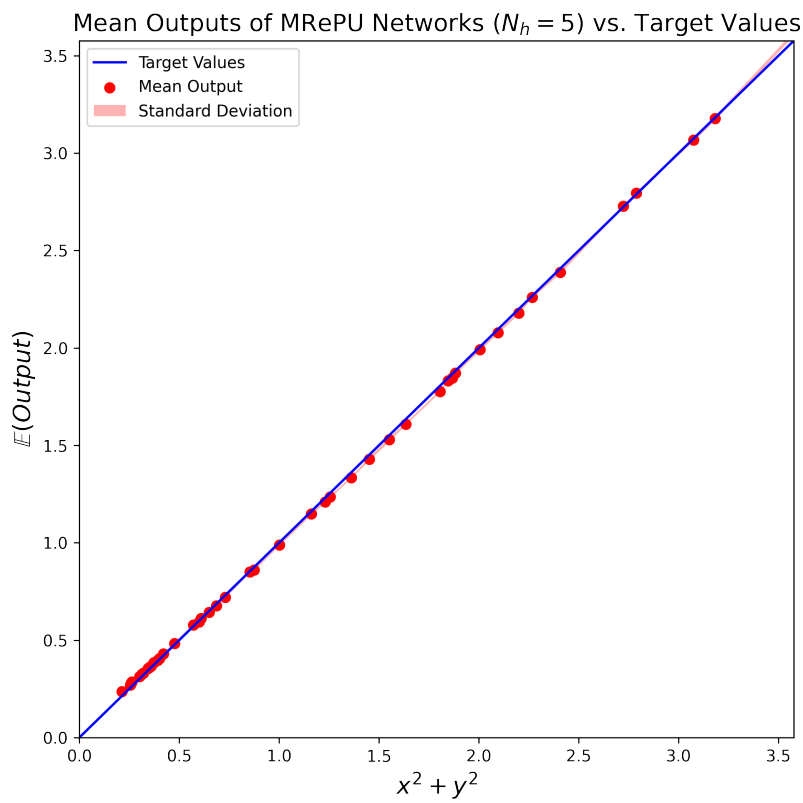


Figure 8: Mean outputs over an ensemble of 100 models versus target values on random test data. The shaded areas represent the region of 1 standard deviation. The number of hidden layers is 5.

5.1 Approximation Theorems for MRePU

In (Shen et al. (2023)), it is shown that a RePU network of p -th order can accurately represent an expanded univariate polynomial using Horner's method, utilizing $4p$ nodes for multiplication and $2p$ nodes to construct a p -th order polynomial. Furthermore, by applying these univariate polynomial results inductively, the representation of multivariate polynomials can also be achieved. Therefore, for the MRePU of order p network, if we can demonstrate that it can construct any p -th order polynomial using $\mathcal{O}(p)$ nodes, as in the case of RePU, we obtain the same result. The following lemma formalizes this.

Lemma 10. A polynomial of degree p , $P(x) = \sum_{k=0}^p a_k x^k$ can be represented by a p -th order MRePU network with one hidden layer and at most $4(p+1)$ hidden nodes.

Proof The proof proceeds in three steps.

Step 1: A 4-unit exact block for $(x - c)^p$ on \mathbb{R} . Fix any $c \in \mathbb{R}$ and write $t := x - c$. Consider the four units

$$\sigma_{m;p}(t-1), \quad \sigma_{m;p}(2t-1), \quad \sigma_{m;p}(-t-1), \quad \sigma_{m;p}(-2t-1).$$

We first compute them on the two half-lines.

Case 1: $t \geq 0$. Then $t-1 \geq -1$ and $2t-1 \geq -1$, while $-t-1 < -1$ and $-2t-1 < -1$. Hence

$$\sigma_{m;p}(t-1) = (t-1)t^p = t^{p+1} - t^p, \quad \sigma_{m;p}(2t-1) = (2t-1)(2t)^p = 2^{p+1}t^{p+1} - 2^p t^p,$$

and $\sigma_{m;p}(-t-1) = \sigma_{m;p}(-2t-1) = 0$. Choose

$$A := -2, \quad B := 2^{-p}.$$

Then

$$\begin{aligned} A\sigma_{m;p}(t-1) + B\sigma_{m;p}(2t-1) &= A(t^{p+1} - t^p) + B(2^{p+1}t^{p+1} - 2^p t^p) \\ &= (A + B2^{p+1})t^{p+1} + (-A - B2^p)t^p \\ &= (-2 + 2^{-p}2^{p+1})t^{p+1} + (2 - 2^{-p}2^p)t^p \\ &= 0 \cdot t^{p+1} + 1 \cdot t^p \\ &= t^p. \end{aligned}$$

Case 2: $t \leq 0$. Then $t-1 < -1$ and $2t-1 < -1$, while $-t-1 \geq -1$ and $-2t-1 \geq -1$. Thus $\sigma_{m;p}(t-1) = \sigma_{m;p}(2t-1) = 0$ and

$$\sigma_{m;p}(-t-1) = (-t-1)(-t)^p = (-t)^{p+1} - (-t)^p,$$

$$\sigma_{m;p}(-2t-1) = (-2t-1)(-2t)^p = 2^{p+1}(-t)^{p+1} - 2^p(-t)^p.$$

With the same A, B as above,

$$\begin{aligned} A\sigma_{m;p}(-t-1) + B\sigma_{m;p}(-2t-1) &= A((-t)^{p+1} - (-t)^p) + B(2^{p+1}(-t)^{p+1} - 2^p(-t)^p) \\ &= (A + B2^{p+1})(-t)^{p+1} + (-A - B2^p)(-t)^p \\ &= 0 \cdot (-t)^{p+1} + 1 \cdot (-t)^p \\ &= (-t)^p. \end{aligned}$$

Since $(-t)^p = (-1)^p t^p$, multiplying by $(-1)^p$ yields

$$(-1)^p (A\sigma_{m;p}(-t-1) + B\sigma_{m;p}(-2t-1)) = t^p.$$

Combining the two cases, for every $t \in \mathbb{R}$ we have the identity

$$t^p = A\sigma_{m;p}(t-1) + B\sigma_{m;p}(2t-1) + (-1)^p (A\sigma_{m;p}(-t-1) + B\sigma_{m;p}(-2t-1)), \quad (12)$$

with $A = -2$ and $B = 2^{-p}$. Substituting $t = x - c$ gives an exact 4-unit one-hidden-layer $\sigma_{m;p}$ -network representation of $(x - c)^p$ on \mathbb{R} .

Step 2: Spanning order p polynomials by shifted p -th powers. Choose distinct real numbers c_0, c_1, \dots, c_p (e.g. $c_i = i$). For each i ,

$$(x - c_i)^p = \sum_{j=0}^p \binom{p}{j} x^j (-c_i)^{p-j}.$$

We claim that for any coefficients (a_0, \dots, a_p) there exist $(\alpha_0, \dots, \alpha_p)$ such that

$$P(x) = \sum_{i=0}^p \alpha_i (x - c_i)^p. \quad (13)$$

Indeed, comparing coefficients of x^j in (13) gives the linear system

$$\sum_{i=0}^p \alpha_i (-c_i)^{p-j} = \frac{a_j}{\binom{p}{j}}, \quad j = 0, 1, \dots, p.$$

The matrix $V = [(-c_i)^{p-j}]_{j,i}$ is a Vandermonde matrix up to a reversal of rows, and since the c_i are distinct it is invertible. Hence the system admits a (unique) solution $(\alpha_0, \dots, \alpha_p)$, proving (13).

Step 3: Assemble the network for P . For each $i \in \{0, \dots, p\}$, represent $(x - c_i)^p$ using the 4-unit identity (12) (with $t = x - c_i$), and multiply the four corresponding output weights by α_i . Summing these $(p+1)$ blocks yields a single one-hidden-layer $\sigma_{m;p}$ network with $4(p+1)$ hidden units whose output equals $\sum_{i=0}^p \alpha_i (x - c_i)^p = P(x)$ for all $x \in \mathbb{R}$.

Therefore any polynomial of degree at most p is represented exactly on \mathbb{R} by a one-hidden-layer p -MRePU network with at most $4(p+1)$ units. \square

Then, by replacing Lemma 40, which is used in the proof of Theorem 3 in (Shen et al. (2023)), we obtain the following theorem:

Theorem 11 If $f : \mathbb{R}^d \rightarrow \mathbb{R}$ is a polynomial of d variables with degree N , then f can be reconstructed via MRePU neural network with depth \mathcal{D} , width \mathcal{W} , number of neurons \mathcal{U} and total number of parameters \mathcal{P} with following specification:

$$\begin{aligned} \mathcal{D} &= 2N - 1, \quad \mathcal{W} = 24(p+1)N^{d-1} + 12(p+1)(N^{d-1} - N)/(N-1) \simeq \mathcal{O}(pN^{d-1}), \\ \mathcal{U} &= (12p+14)(2N^d - N^{d-1} - N) + (4p+4)(2N^d - N^{d-1} - N)/(N-1) \simeq \mathcal{O}(pN^d), \\ \mathcal{P} &= (60p+62)(2N^d - N^{d-1} - N) + (4p+5)(2N^d - N^{d-1} - N)/(N-1) \simeq \mathcal{O}(pN^d). \end{aligned}$$

Additionally, as a corollary to the above theorem, we obtain a universal approximation result for the class of differentiable functions, which corresponds to Theorem 5 in (Shen et al. (2023)). Before stating this result, we define a reference norm that will serve as our standard.

Definition 12. We define the norm of $f \in C^s(A)$, where $A \subset \mathbb{R}^d$, as following:

$$\|f\|_{C^s} := \sum_{|\alpha| \leq s} \sup_{x \in A} |D^\alpha f(x)|,$$

where α is an index vector for partial derivative and $|\alpha|$ is total order of derivative.

Corollary 13. Let f be a function belongs to $C^s(K)$ where $K \subset \mathbb{R}^d$ is a compact set. For any $N \in \mathbb{N}^+$, there exists a MRePU neural network ψ_N with depth \mathcal{D} , width \mathcal{W} , number of neurons \mathcal{U} and total number of parameters \mathcal{P} with following specification:

$$\begin{aligned} \mathcal{D} &= 2N - 1, & \mathcal{W} &= 24(p+1)N^{d-1} + 12(p+1)(N^{d-1} - N)/(N-1) \simeq \mathcal{O}(pN^{d-1}), \\ \mathcal{U} &= (12p+14)(2N^d - N^{d-1} - N) + (4p+4)(2N^d - N^{d-1} - N)/(N-1) \simeq \mathcal{O}(pN^d), \\ \mathcal{P} &= (60p+62)(2N^d - N^{d-1} - N) + (4p+5)(2N^d - N^{d-1} - N)/(N-1) \simeq \mathcal{O}(pN^d). \end{aligned}$$

where $C_{p,s,d,K}$ is a positive constant which depends only on p, d, s and the diameter of K .

5.2 Experiments on Synthetic Data

In this section, we experimentally confirm that the MRePU network, by restricting the hypothesis class and thus providing inductive bias, achieves faster convergence of training loss compared to networks constructed with conventional activations such as ReLU or GELU. RePU is excluded from the comparison group as stacking layers with it is entirely infeasible.

Regression on polynomials and differentiable functions First, we validate the efficiency of MRePU on polynomial functions. The neural network architecture consists of five hidden layers, each with a width of 32, and the input dimension is set according to the variables in each polynomial. For univariate polynomial problems, the training dataset was constructed with inputs from -2.0 to 2.0, divided into 101 points at intervals of 0.04. For $x^3 - x$, the learning rate was set to 0.005, and C_W was set to 0.5 for MRePU and 1.0 for other cases. For $x^5 - 5x^3 + 6x$, the learning rate was set to 0.0001, with C_W set to 0.8 for MRePU case and learning rate to 0.001, C_W to 1.0 for the others. For multivariate cases, the dataset for xy was created by forming a meshgrid over the range $[-2, 2] \times [-2, 2]$, with each axis divided into 101 points. Similarly, for xyz , a meshgrid was formed over the range $[-1, 1] \times [-1, 1] \times [-1, 1]$, with each axis divided into 51 points. Training was conducted up to 10,000 epochs for all cases. The learning rate for multivariate cases was set to 0.001, and C_W was set to 0.55 for xy , 0.6 for xyz , and 1.0 for the other cases. Each hyperparameter was empirically determined to achieve optimal performance. Table 4 presents the average final loss over 25 experiments, where neural networks were trained to regress each polynomial function. As observed in the table, MRePU-based neural networks consistently outperform the others in all cases. Notably, for approximating xyz , other networks fail to learn effectively, while only the MRePU network achieves meaningful learning. The loss plots for $x^5 - 5x^3 + 6x$ and xy are depicted in Fig. 9. Fig. 10 illustrates the regression

	$x^3 - x$	$x^5 - 5x^3 + 6x$	xy	xyz
MRePU	4.0×10^{-4}	2.0×10^{-4}	2.7×10^{-5}	2.5×10^{-4}
ReLU	8.0×10^{-4}	7.0×10^{-4}	4.0×10^{-4}	4.2×10^{-2}
GELU	7.2×10^{-2}	2.1×10^{-3}	4.0×10^{-4}	4.2×10^{-2}

Table 4: Mean final training losses over 25 trials for polynomial approximation for each of the MRePU (order $p = 2$), ReLU, and GELU networks. The values in bold represent the lowest values in each column.

results of $x^5 - 5x^3 + 6x$ using ReLU and MRePU. A key observation is that the trained MRePU network approximates not only the function itself but also its derivative, whereas the ReLU network produces a piecewise function with noticeable discontinuities. Similarly, Fig. 11 shows the contour graphs of trained networks with different activation functions for xy . The MRePU network demonstrates a highly accurate approximation, while the ReLU network exhibits significant instability in the contours, and GELU shows reduced accuracy.

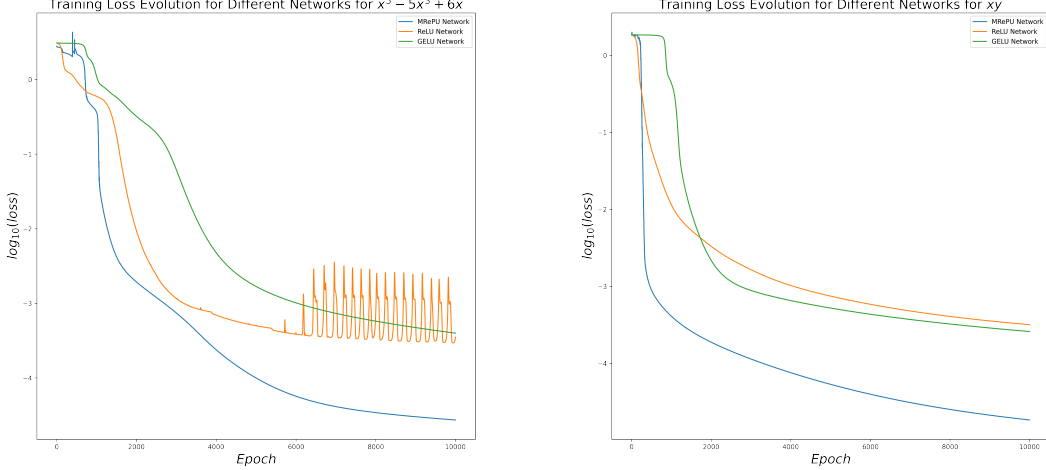


Figure 9: The training loss plots for each neural network over epochs for the cases of $x^5 - 5x^3 + 6x$ (**Left**) and xy (**Right**).

Next, we conducted experiments on differentiable functions. The neural network architecture remained identical to that used for polynomial regression. The experiments involved

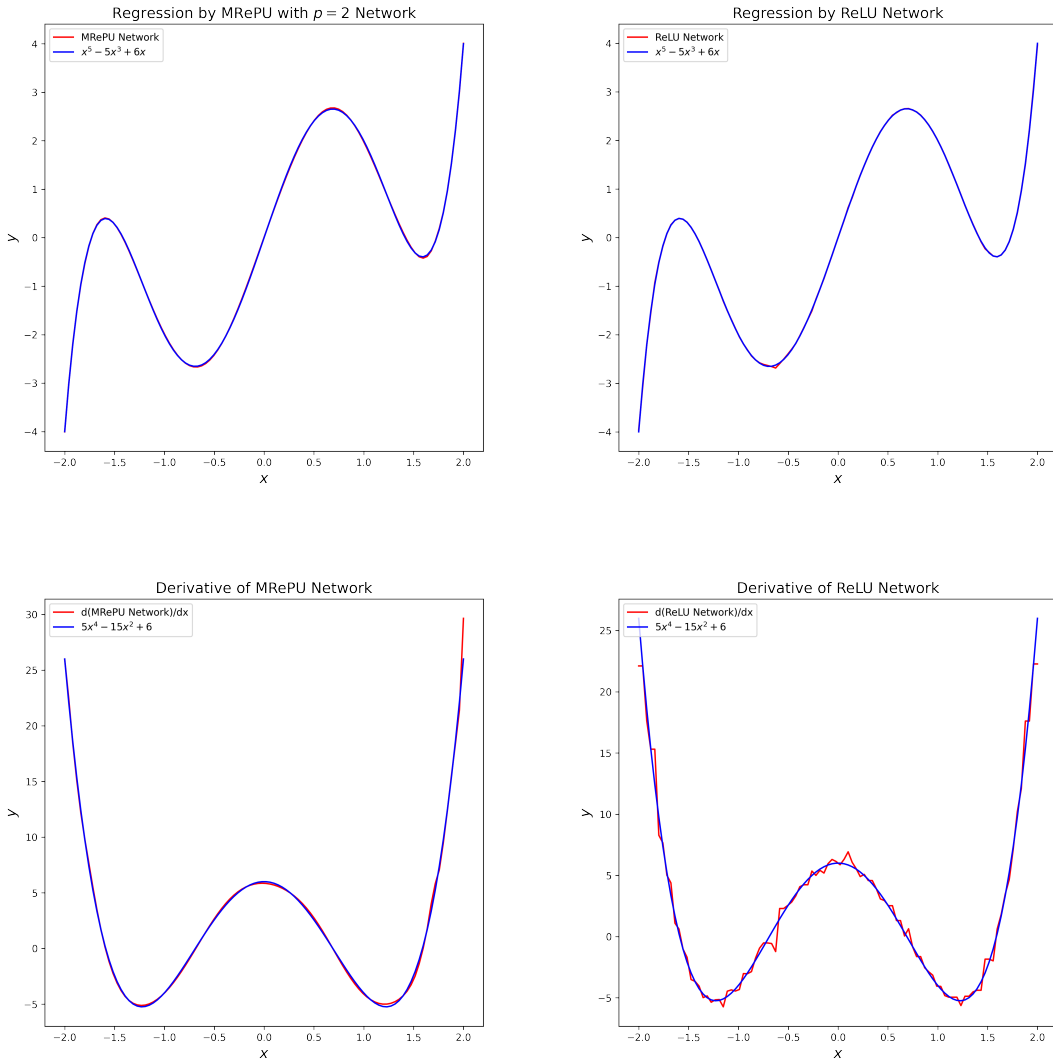


Figure 10: **Top:** The results of training for regressing $x^5 - 5x^3 + 6x$, where the left plot shows the output of the MRePU with $p = 2$ network, and the right plot shows the output of the ReLU network. **Bottom:** The comparison between the derivative of the trained networks and the actual derivative function, $5x^4 - 15x^2 + 6$.

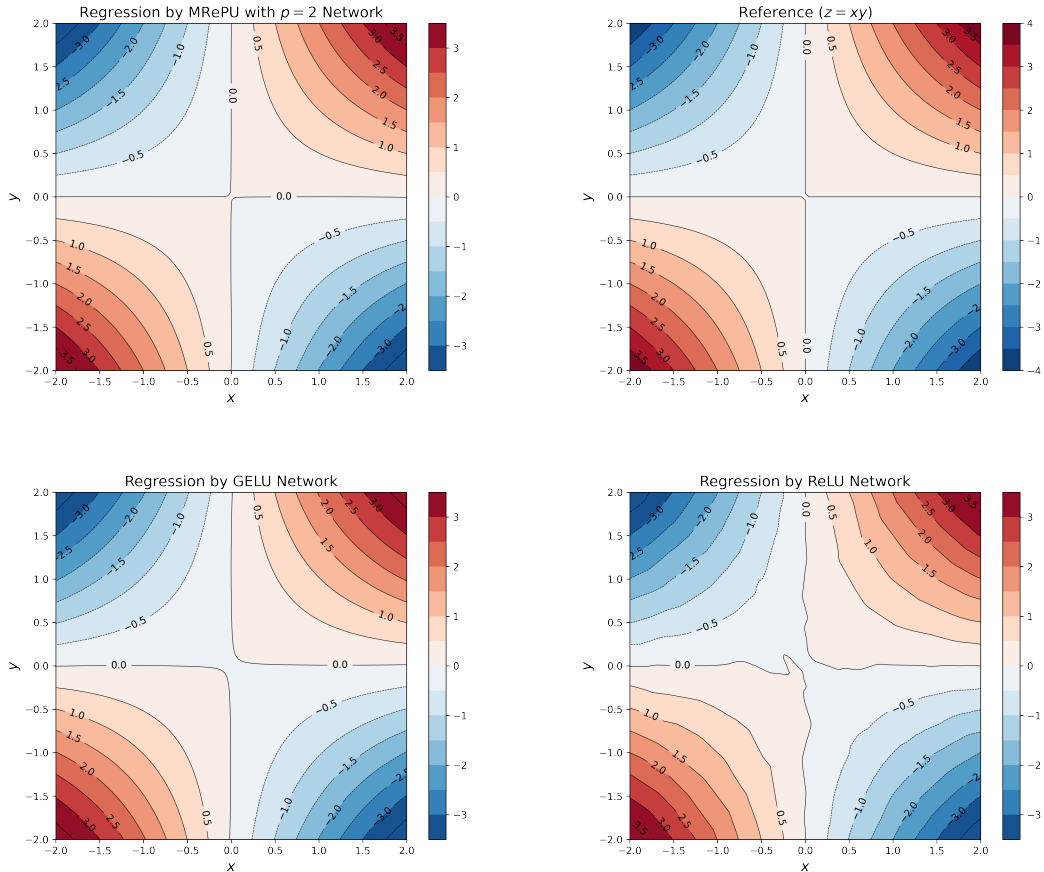


Figure 11: Contour plots for the reference function and the trained neural networks. **Top left:** MRePU with $p = 2$ network. **Top right:** Reference (xy). **Bottom left:** GELU network. **Bottom right:** ReLU network.

regression on $\lfloor x \rfloor_+^3$ and the functions $f(x)$ and $g(x, y)$, defined as follows.

$$f(x) = \begin{cases} x^4 - 3x^2 + 1 & \text{if } x \leq -1 \\ -x^2 & \text{if } -1 \leq x \leq 0 \\ x^3 & \text{if } 0 \leq x \leq 1 \\ 3x - 2 & \text{if } 1 \leq x \end{cases}$$

$$g(x, y) = \begin{cases} 10(r^2 - \frac{1}{2})^2 & \text{if } r \leq \frac{1}{\sqrt{2}} \\ (r^2 - \frac{1}{2})^3 & \text{otherwise} \end{cases}$$

$$r = \sqrt{x^2 + y^2}$$

The training dataset for univariate functions was constructed in the same manner as for the polynomials. For multivariate functions, a meshgrid was generated by dividing the domain $[-1, 1] \times [-1, 1]$ into 51 intervals along each axis. The learning rate and C_W values for these experiments were as follows: For $\lfloor x \rfloor_+^3$, the MRePU network used a learning rate of 0.0004 and $C_W = 0.6$, while the other networks used 0.001 and $C_W = 1.0$. For $f(x)$, The MRePU network employed a learning rate of 0.001 and $C_W = 0.6$, while the other networks used 0.001 and $C_W = 1.0$. For $g(x, y)$, the MRePU network used a learning rate of 0.002 and $C_W = 0.8$, whereas the remaining networks used 0.003 and $C_W = 1.0$. Each hyperparameter was empirically determined to achieve optimal performance.

	$\lfloor x \rfloor_+^3$	$f(x)$	$g(x, y)$
MRePU	8.1×10^{-5}	7.9×10^{-5}	4.0×10^{-4}
ReLU	3.2×10^{-5}	5.6×10^{-5}	2.0×10^{-4}
GELU	2.4×10^{-3}	8.0×10^{-4}	4.4×10^{-1}

Table 5: Mean final training losses over 25 trials for the approximation of differentiable functions for each of the MRePU (order $p = 2$), ReLU, and GELU networks. The values in bold represent the lowest values in each column.

As shown in Table 5 and Fig. 12, for differentiable functions with discontinuities in higher-order derivatives, the ReLU network generally demonstrates the best performance. However, as observed in Figs. 13 and 14, even though the training loss of the ReLU network is lower (i.e., its L^2 norm is smaller), the MRePU network exhibits more stable function approximation in terms of contour smoothness and the behavior of the differentiated function. For the GELU network, it is evident that learning fails entirely for $g(x, y)$.

Case of Physics-Informed Neural Networks (PINNs) Next, we compare and contrast neural networks constructed with different activation functions using the physics-informed neural networks (PINNs) (Raissi et al. (2019)) technique, which solves PDE problems by incorporating the PDE itself into the loss function. The PDE used in this experiment is the Burgers equation, given as:

$$\frac{\partial u}{\partial t} + u \frac{\partial u}{\partial x} = \nu \frac{\partial^2 u}{\partial x^2}$$

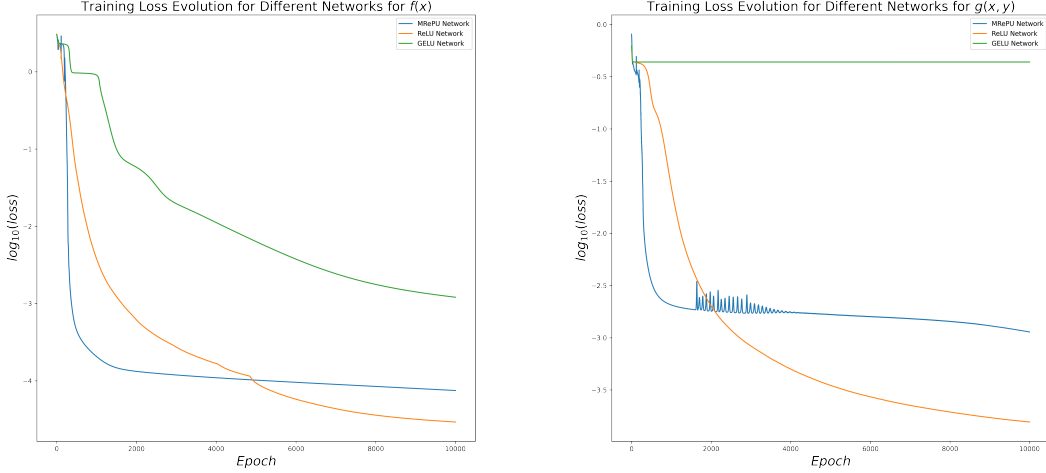


Figure 12: The training loss plots for each neural network over epochs for the cases of $f(x)$ (Left) and $g(x, y)$ (Right).

We defined the problem domain as $(x, t) \in [-1, 1] \times [0, 1]$ with $\nu = \frac{0.01}{\pi}$. The initial condition (the function value at $t = 0$) was set to $-\sin \pi x$, and the boundary condition was defined as $u(-1, t) = u(1, t) = 0$. The PINN loss comprises the L^2 loss for the boundary condition and the loss for the PDE. The number of points used for loss calculations was as follows: 10,000 randomly sampled collocation points within the domain and 100 points for the boundary condition. The hyperparameter settings included the use of the Adam optimizer with a learning rate of 0.001, betas set to $(0.9, 0.999)$, and weight decay set to 0. For C_W , the value was set to 0.45 for MRePU with $p = 2$ and 1.0 for all other cases. The neural network architecture was consistent across experiments, with an input dimension of 2, seven hidden layers, and a width of 64 per layer.

The results of the experiment are presented in Fig. 15, 16, and 17. Interestingly, unlike the previous cases with polynomials and differentiable functions, the GELU activation exhibited the best performance, followed by the MRePU network. The ReLU network, however, failed to achieve meaningful learning. Additional experiments with the Tanh activation showed a performance similar to that of the GELU network. From this experiment, it can be concluded that the MRePU network is capable of achieving meaningful learning even under the highly complex training dynamics of the PINN loss (Wang et al. (2022), Krishnapriyan et al. (2021)) and with a deep architecture consisting of 7 hidden layers (9 layers in total).

To conclude the results of the experiments, it was observed that the characteristics of each activation function (piecewise linear, differentiable, smooth) introduced an inductive bias to the neural network architecture, affecting its effectiveness in approximating specific function classes. These classes included polynomial functions, differentiable functions, and solutions to PINNs (generally smooth functions). Depending on the nature of the task,

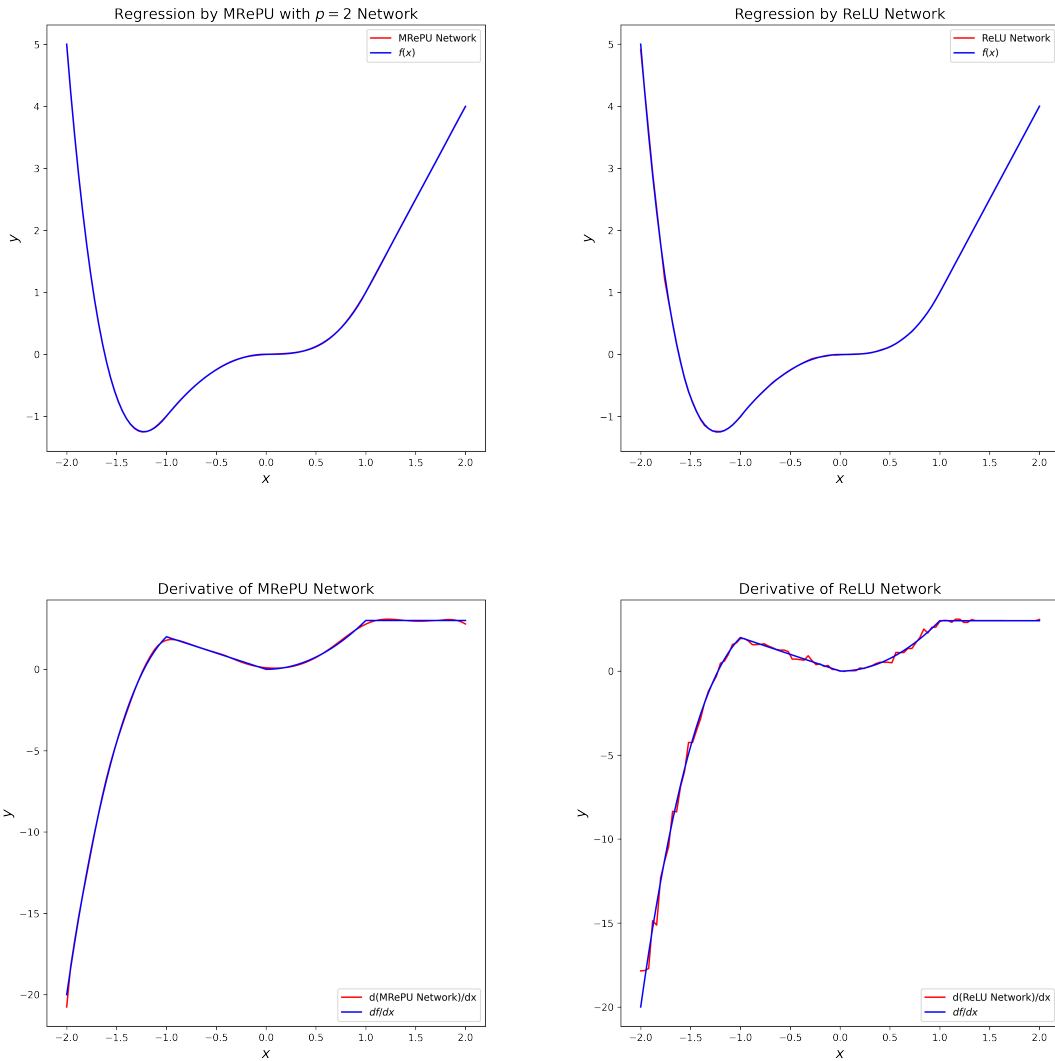


Figure 13: **Top:** The results of training for regressing $f(x)$, where the left plot shows the output of the MRePU with $p = 2$ network, and the right plot shows the output of the ReLU network. **Bottom:** The comparison between the derivative of the trained networks and the actual derivative function.

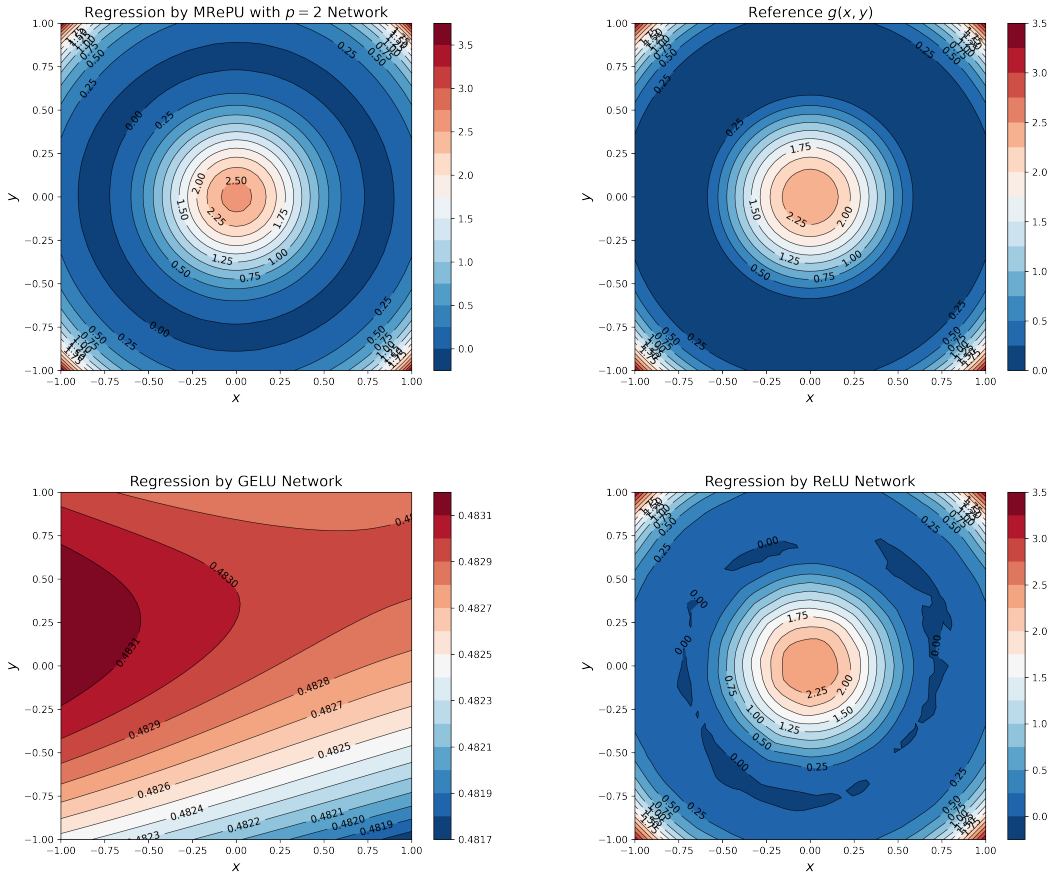


Figure 14: Contour plots for the reference function and the trained neural networks. **Top left:** MRePU with $p = 2$ network. **Top right:** Reference $(g(x, y))$. **Bottom left:** GELU network. **Bottom right:** ReLU network.

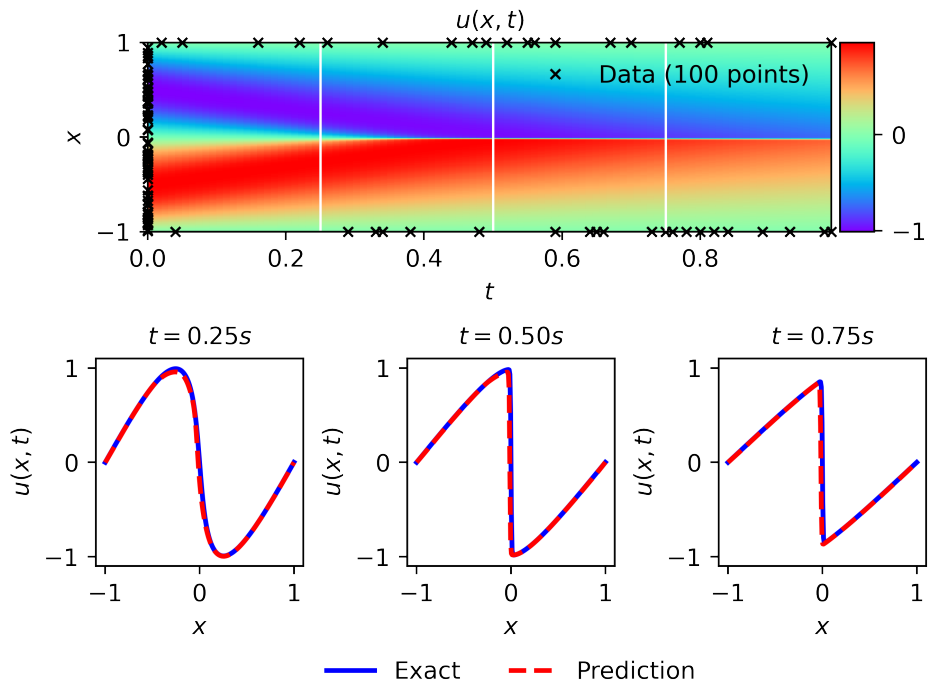


Figure 15: The PINN training results of the MRePU with $p = 2$ network. **Top:** The learned neural network function represented as a heatmap over the entire domain. **Bottom:** Plots of the function cross-sections at $t = 0.25$, $t = 0.50$, and $t = 0.75$.

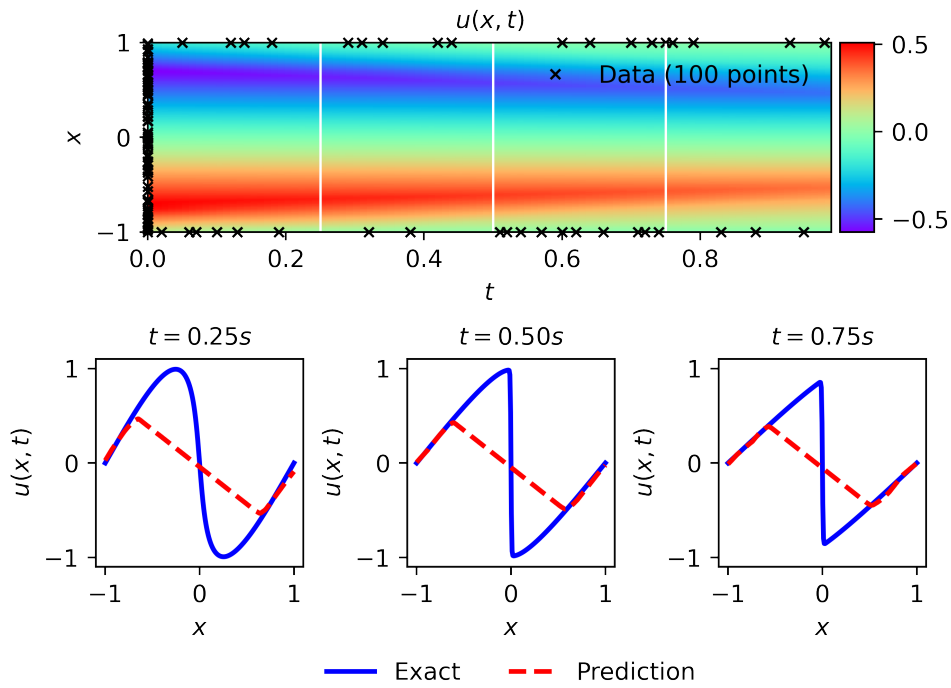


Figure 16: The PINN training results of the ReLU network. **Top:** The learned neural network function represented as a heatmap over the entire domain. **Bottom:** Plots of the function cross-sections at $t = 0.25$, $t = 0.50$, and $t = 0.75$.

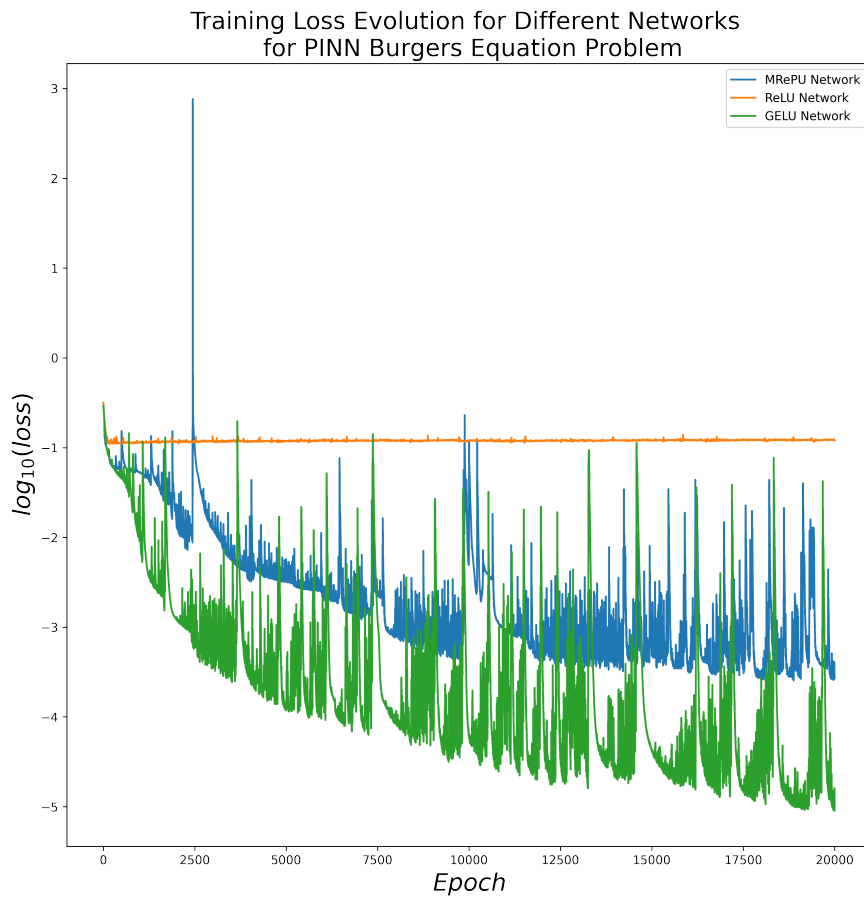


Figure 17: The training loss plots for each neural network over epochs for the case of Burgers equation PINN problem.

certain activation functions and architectures were found to be more effective, while others were not. The effectiveness of each activation function, based on the training loss, is summarized as follows:

Polynomial: MRePU > ReLU* > GELU*
Differentiable function: ReLU > MRePU** > GELU*
PINN for Burgers equation: GELU > MRePU > ReLU*

Here, the * symbol indicates cases where the training either fails entirely or is effective only under specific conditions. Additionally, the ** symbol denotes the best effectiveness when considering derivatives as well.

5.3 Experiments on Real-World Data

In this section, we extend our experiments beyond synthetic data to real-world datasets, specifically MNIST and CIFAR-10. Consistent with the setup in Section 5.2, we trained neural network architectures employing MRePU, ReLU, and GELU activation functions. A particularly notable observation in this section is that MRePU networks can be directly applied to very deep neural networks and the widely used ResNet architecture with only minor modifications.

MNIST Classification First, we conducted experiments on the MNIST dataset, which is fundamental and widely used for verification. The 28×28 input images were flattened into 784-dimensional vectors, and a 4-layer FCN architecture with dimensions [784, 256, 256, 256, 10] was employed. In all experiments, training was performed using the Adam optimizer with a learning rate of 10^{-3} . For the first experiment verifying the criticality condition, a batch size of 512 was used, while in the second experiment comparing the performance of various activation functions, a batch size of 64 was utilized. In the first experiment, to empirically demonstrate that the condition in Eq. (11) serves as a boundary condition for training stability, the dataset was centered and scaled by dividing by N_K (ranging from 0.1 to 2.0 with an interval of 0.1). Similarly, the hyperparameter C_W was varied from 0.1 to 2.0 with an interval of 0.1. We performed training for 5 epochs for each case, repeated the process 10 times, and visualized the average test accuracy as a heatmap (Fig. 18). By regarding C_W in Eq. (11) as a function $\tilde{C}_W(K)$ of K for the case where $p = 2$, the criticality condition or phase boundary obtained via fitting form of function $a\tilde{C}_W(b/N_K)$ into $2.2\tilde{C}_W(0.02/N_K)$, is depicted as a dotted red line in Fig. 18. As shown in the figure, the success of neural network training is highly sensitive to C_W , and the fitted threshold condition aligns well with the empirical observations. Notably, as N_K increases and the data approaches the fixed point $K^* = 0$, the sensitivity to C_W diminishes.

In the second experiment, for each activation function, the dataset was centered and normalized by dividing by $N_K = 30$ to ensure proximity to the fixed point. The training process was conducted for 10 epochs and repeated 25 times. The average test loss and accuracy are presented in Table 6, while the training loss, plotted on a logarithmic scale with a 50-iteration moving average, is displayed in the left panel of Fig. 19. As illustrated in Fig. 19, MRePU demonstrates rapid convergence in the initial phase, followed by a convergence rate comparable to that of ReLU. Furthermore, the results in Table 6 indicate that all tested activation functions exhibit similar performance.

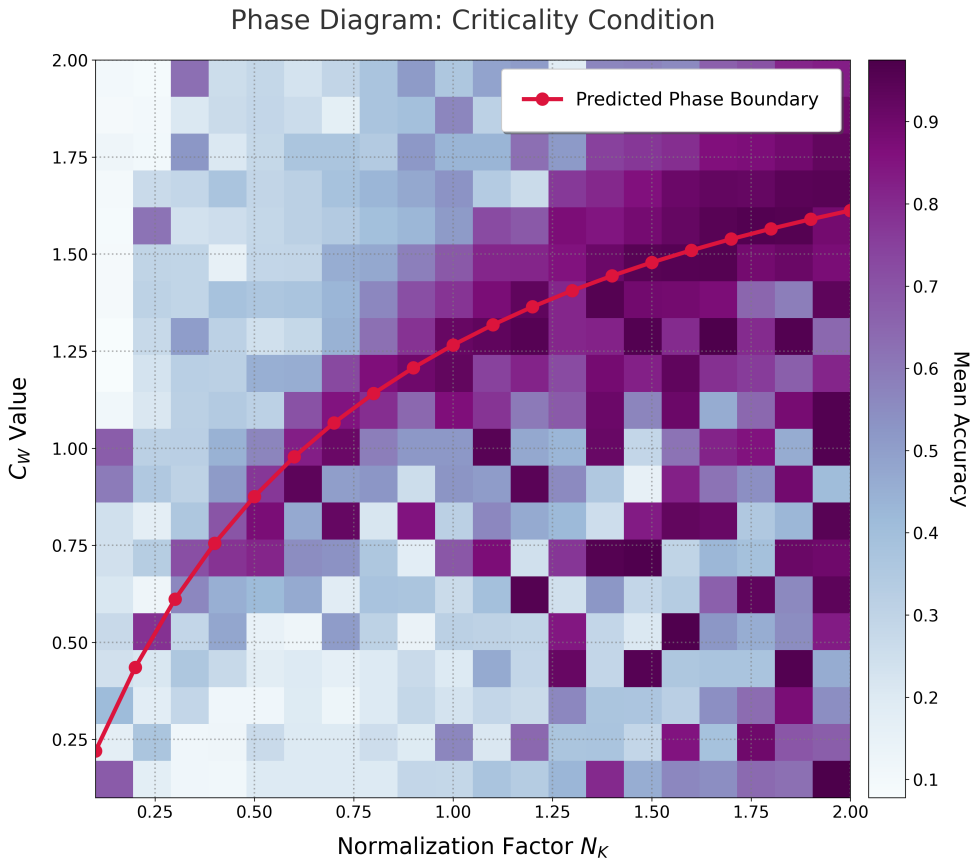


Figure 18: Phase diagram illustrating the criticality condition of the hyperparameter C_W with respect to the normalization factor N_K . The background heatmap represents the empirical mean accuracy obtained from 10 training results, where purple indicates higher performance. The overlaid red solid line denotes the theoretical phase boundary derived from Proposition 8, demonstrating a strong alignment with the empirical transition region.

CIFAR-10 Classification For the CIFAR-10 dataset, we employed the ResNet architecture. For ReLU and GELU, we adhered to the architecture described in (He et al. (2016)), utilizing the basic building block. The network is constructed by arranging blocks with widths of 64, 128, 256, and 512 in a sequence of 2, 2, 1, and 1 blocks, respectively. Each block consists of two 3×3 convolutional layers with a residual connection added to the input and output. Including the input and output layers, the total depth of the architecture is $1 + 2(2 + 2 + 1 + 1) = 14$ layers.

For MRePU, we modified the residual structure as follows, which is an essential adjustment to maintain the kernel at a constant scale (Roberts et al. (2022)):

$$z^{(l+1)} = \gamma \text{Block}(z^{(l)}) + \sqrt{1 - \gamma^2} z^{(l)}$$

where $z^{(l+1)}$ is final output of whole block and $z^{(l)}$ is input of the block $0 < \gamma < 1$ is a weight for the residual term. Since MRePU, ReLU, and GELU all share $K^* = 0$ as a fixed point, it is fair to ensure the kernel scale remains close to zero. Consequently, we normalized the dataset to the following scale, where scaling factor in denominator is empirically tuned:

$$X^* = \frac{X - \mathbb{E}[X]}{5000}$$

We utilized a batch size of 64 and the Adam optimizer with a learning rate of 2.5×10^{-4} . The training was conducted for 5 epochs. We performed a total of 25 independent trials for each activation function, and the average test loss and accuracy are reported in Table 6. The moving average of the log-scaled training loss, calculated over a window of 50 iterations, is depicted in the right panel of Fig. 19. While all three activation functions exhibit similar trends, it is observed that, unlike in the MNIST case, the reduction in training loss for MRePU lags slightly behind the others. Although the training-loss curves exhibit qualitatively similar trends across activations, MRePU (with $p = 2$) yields a noticeably higher test loss and lower test accuracy on CIFAR-10 (Table 6). Nevertheless, the main significance of MRePU lies in enabling stable optimization in deeper and more complex architectures such as ResNets under the proposed criticality condition. In our experiments, such stable training was not observed when using RePU, or when the criticality condition was violated, where optimization frequently became unstable and failed to converge.

	MNIST		CIFAR-10	
	Loss	Accuracy	Loss	Accuracy
MRePU	1.8×10^{-2}	97.7%	1.29	57.7%
ReLU	1.3×10^{-2}	98.4%	7.53×10^{-1}	72.4%
GELU	2.0×10^{-2}	98.0%	7.71×10^{-1}	67.4%

Table 6: Mean final test losses and accuracies over 25 trials for real-world tasks for each of the MRePU (order $p = 2$), ReLU, and GELU networks. The values in bold represent the lowest test loss values(highest for accuracies) in each column.

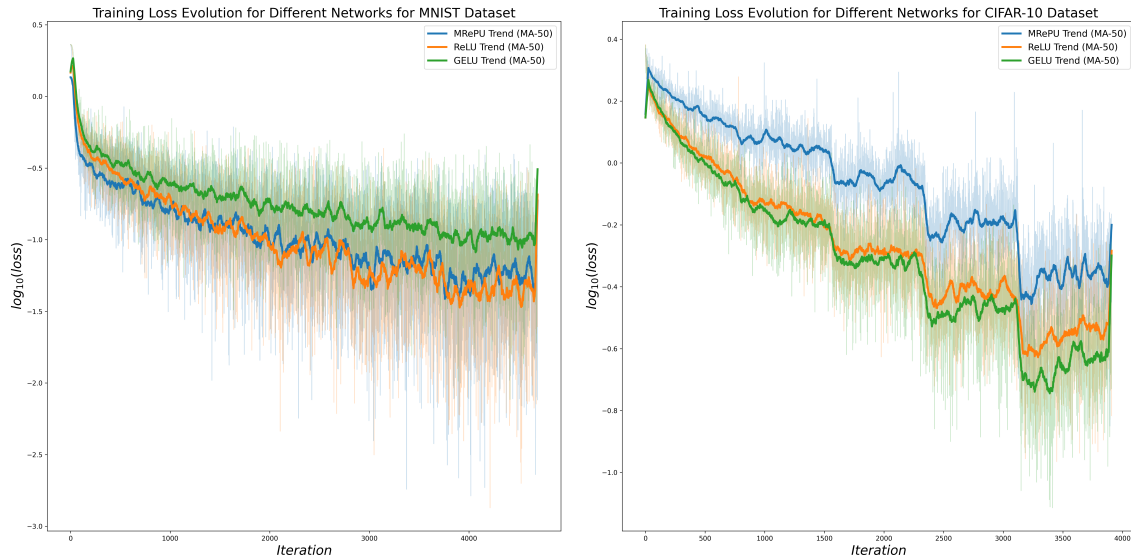


Figure 19: The training loss plots for each neural network over epochs for the cases of MNIST (**Left**) and CIFAR-10 (**Right**) datasets.

6. Conclusion

In this paper, we analyzed neural networks using Effective Field Theory to theoretically predict and experimentally verify the failure of deep neural network architectures employing RePU activation. Furthermore, we proposed the Modified Rectified Power Unit (MRePU) activation function to address the limitations of RePU and provided a theoretical estimation of its effectiveness. We then empirically validated its feasibility by comparing experimental results with theoretical predictions.

The proposed MRePU demonstrated the ability to facilitate learning even in deep networks. Mathematically, we confirmed that MRePU retains the favorable properties of RePU, such as p -differentiability and universal approximation capabilities. This suggests that the beneficial characteristics identified in previous studies on RePU can be extended to MRePU. Moreover, MRePU introduces a specific inductive bias into deep neural networks, thereby enabling effective learning when approximating functions within a specific differentiability class.

We also verified that the derived criticality condition aligns well with empirical validation on the MNIST dataset, a standard benchmark in computer vision, proving the effectiveness of MRePU in terms of both the stability of training dynamics near the fixed point and test accuracy. Furthermore, we extended our experiments to the more challenging CIFAR-10 task using a 14-layer ResNet architecture. While RePU activation failed to train at this depth, MRePU successfully demonstrated the capability to train on such deep and complex datasets.

References

A. Abdeljawad and P. Grohs. Integral representations of shallow neural network with rectified power unit activation function. *Neural Networks*, 155:536–550, 2022.

I. Banta, T. Cai, N. Craig, and Z. Zhang. Structures of neural network effective theories. *Phys. Rev. D*, 109:105007, 2024.

C. M. Bishop. *Pattern Recognition and Machine Learning*. Springer New York, NY, 2006.

DA. Clevert, T. Unterthiner, and S. Hochreiter. Fast and accurate deep network learning by exponential linear units (elus). *International Conference on Learning Representations (ICLR)*, 2015.

G. Cybenko. Approximation by superpositions of a sigmoidal function. *Mathematics of Control and Signals and Systems*, 2:303–315, 1989.

W. E and B. Yu. The deep ritz method: A deep learning-based numerical algorithm for solving variational problems. *Communications in Mathematics and Statistics*, 6:1–12, 2018.

X. Glorot, A. Bordes, and Y. Bengio. Deep sparse rectifier neural networks. *Proceedings of the 14th International Conference on Artificial Intelligence and Statistics (AISTATS)*, 2011.

J. Halverson, A. Maiti, and K. Stoner. Neural networks and quantum field theory. *Mach. Learn.: Sci. Technol.*, 2:035002, 2021.

K. He, X. Zhang, S. Ren, and J. Sun. Delving deep into rectifiers: Surpassing human-level performance on imagenet classification. *Proceedings of the IEEE International Conference on Computer Vision (ICCV)*, 2015.

K. He, X. Zhang, S. Ren, and J. Sun. Deep residual learning for image recognition. *Proceedings of the IEEE Conference on Computer Vision and Pattern Recognition (CVPR)*, 2016.

D. Hendrycks and K. Gimpel. Gaussian error linear units (gelus). *Arxiv*, 2016.

Aditi S. Krishnapriyan, Amir Gholami, Shandian Zhe, Robert M. Kirby, and Michael W. Mahoney. Characterizing possible failure modes in physics-informed neural networks. *Proceedings of the Neural Information Processing Systems Conference (NeurIPS)*, 2021.

Y. A. LeCun, L. Bottou, G. B. Orr, and KR Müller. *Efficient BackProp*. Springer, Berlin, 2002.

B. Li, S. Tang, and H. Yu. Powernet: Efficient representations of polynomials and smooth functions by deep neural networks with rectified power units. *J. Math. Study*, 53:159–191, 2020.

A. L. Maas, A. Y. Hannun, and A. Y. Ng. Rectifier nonlinearities improve neural network acoustic models. *Proceedings of the 30th International Conference on Machine Learning (ICML)*, 2013.

V. Nair and G. E. Hinton. Rectified linear units improve restricted boltzmann machines. *Proceedings of the 27th International Conference on Machine Learning (ICML)*, 2010.

S. Narayan. The generalized sigmoid activation function: Competitive supervised learning. *Information Sciences*, 99(1-2):69–82, 1997.

R. M. Neal. *Bayesian Learning for Neural Networks*. Springer New York, NY, 1996.

G. Parascandolo, H. Huttunen, and T. Virtanen. Taming the waves: sine as activation function in deep neural networks. *Arxiv*, 2016.

M. Raissi, P. Perdikaris, and G.E. Karniadakis. Physics-informed neural networks: A deep learning framework for solving forward and inverse problems involving nonlinear partial differential equations. *Journal of Computational Physics*, 378:686–707, 2019.

P. Ramachandran, B. Zoph, and Q. V. Le. Searching for activation functions. *Arxiv*, 2017.

C. E. Rasmussen. *Gaussian Processes in Machine Learning*. Springer, Berlin, 2004.

D. A. Roberts, S. Yaida, and B. Hanin. *The Principles of Deep Learning Theory*. Cambridge University Press, 2022.

F. Rosenblatt. The perceptron: A probabilistic model for information storage and organization in the brain. *Psychological Review*, 65(6):386–408, 1958.

D. E. Rumelhart, G. E. Hinton, and R. J. Williams. Learning representations by back-propagating errors. *Nature*, 323:533–536, 1986.

G. Shen, Y. Jiao, Y. Lin, , and J. Huang. Differentiable neural networks with repu activation: with applications to score estimation and isotonic regression. *Arxiv*, 2023.

V. Sitzmann, J. N. P. Martel, A. W. Bergman, D. B. Lindell, and G. Wetzstein. Implicit neural representations with periodic activation functions. *Proceedings of the Neural Information Processing Systems Conference (NeurIPS)*, 2020.

H. Sun, Z. Wu, B. Xia, P. Chang, Z. Dong, Y. Yuan, Y. Chang, and X. Wang. A method on searching better activation functions. *Arxiv*, 2024.

Sifan Wang, Xinling Yu, and Paris Perdikaris. When and why pinns fail to train: A neural tangent kernel perspective. *Journal of Computational Physics*, 449:110768, 2022.